In-Vivo Studies of New Vector Velocity and Adaptive Spectral Estimators in Medical Ultrasound

Kristoffer Lindskov Hansen

This review has been accepted as a thesis together with four previously published papers by University of Copenhagen, September 9, 2009, and defended on February 29, 2010.

Tutors: Michael Bachmann Nielsen, Jørgen Arendt Jensen

Official opponents: Liselotte Højgaard, Hans Nygaard, Ola Bjorgell

Correspondance: Department of Radiology, Rigshospitalet, Blegdamsvej 9, DK-2200 Copenhagen

E-mail: kristofferhansen@hotmail.com

Dan Med Bull 2010; 57: B4143

ABSTRACT: New ultrasound techniques for blood flow estimation have been investigated in-vivo. These are vector velocity estimators (Transverse Oscillation, Synthetic Transmit Aperture, Directional Beamforming and Plane Wave Excitation) and adaptive spectral estimators (Blood spectral Power Capon and Blood Amplitude and Phase Estimation). It was shown that the vector velocity estimators can provide reliable angle independent estimates and new insight to the complexity of blood flow, and that adaptive spectral estimators can produce useful spectrograms faster than the conventional spectral Doppler method.

INTRODUCTION

In this PhD project new ultrasound techniques for blood flow measurements have been investigated *in-vivo*. The focus has mainly been on vector velocity techniques and four different approaches have been examined: Transverse Oscillation (TO), Synthetic Transmit Aperture (STA), Directional Beamforming (DB) and Plane Wave Excitation (PWE). Furthermore, two different adaptive spectral estimators have been investigated: Blood spectral Power Capon method (BPC) and Blood Amplitude and Phase Estimation method (BAPES).

The studies were focused on evaluations of new methods for blood flow measurements. The methods have previously been evaluated in simulations and in flow phantoms. This work concerns *in-vivo* validation, which is an important investigational stage before any new method can be implemented into commercial scanners. The methods are all thought as possible solutions to some of the inherent limitations found in conventional Doppler ultrasound. Firstly, modern scanners of today can only estimate blood velocities angle dependently and this introduces an operator dependent angle correction. The angle correction is build upon the assumption of laminar flow, which is a gross simplification. Secondly, the frame rate of the B-mode images and the temporal resolution of the velocity estimation suffer when several ultrasound modalities are performed simultaneously as in duplex and triplex scan mode.

Transverse Oscillation, Synthetic Transmit Aperture and Directional Beamforming can estimate the blood velocity angle independently. The three methods were validated *in-vivo* against magnetic resonance phase contrast angiography when measuring stroke volumes in simple vessel geometry on 11 volunteers. Using linear regression and Bland-Altman analyses good agreements were found, indicating that vector velocity methods can be used for quantitative blood flow measurements.

Plane Wave Excitation can estimate blood velocities angle independently with a high frame rate. Complex vessel geometries in the cardiovascular system were explored *in-vivo* on four volunteers using the technique. Flow patterns previously visualized with magnetic resonance angiography and predicted by models of computational fluid dynamics, were shown for the first time with ultrasound. Additionally, new information on complex flow patterns in bifurcations and around venous valves was discovered.

BPC and BAPES are adaptive spectral estimators, which can produce spectrograms with a high temporal resolution. Spectrograms obtained *in-vivo* with the two techniques on ten volunteers were evaluated quantitatively and qualitatively and compared to the conventional spectral Doppler method. Descriptive statistics, kappa statistics and multiple t-tests were performed and it was shown that BAPES and BPC can produce useful spectrograms with a narrower observation window compared to the conventional spectral Doppler method.

The angle independent vector velocity estimators and fast adaptive spectral estimators were investigated using the experimental scanner RASMUS (Remotely Accessible Software configurable Multi-channel Ultrasound Sampling) (1;2). RASMUS made it possible to realize the *in-vivo* clinical trials as full control was achieved of how signals were sent out and how the scattered signals were received.

The thesis shows, that novel information can be obtained with vector velocity methods providing quantitative estimates of blood flow and insight in to the complexity of fluid dynamics. This could give the clinician a new tool in assessment and treatment of cardiovascular diseases. Also solutions to produce spectrograms with fewer emissions per estimate were given. This could potentially bring improvements to spectral blood estimation as an increase of the temporal resolution of the spectrogram or as an increase of the frame rate for the interleaved B-mode images.

BACKGROUND

Definition of blood flow

Blood flow is defined as the flow of blood in the cardiovascular system. Flow can be described as laminar, disturbed/complex or turbulent flow. The transition of flow from laminar to turbulent is dependent on a number of factors, e.g. vessel geometry, velocity, pulsation and plaque involvement. In healthy individuals only laminar and disturbed/complex flow patterns are present while turbulent flow is a symptom of vessel disease. The type of flow is described numerically by the Reynolds number and usually turbulence occurs when the Reynolds number exceeds 2500 (3). Flow can be measured as a velocity (meters per second) or a quantity (liters per second or liters per stroke). Flow measurements can be done invasively or non-invasively. In this thesis are only used non-invasive methods for blood flow estimation. Nevertheless, a brief introduction to some of the invasive methods is presented below.

Invasive techniques

Invasive techniques for measuring blood flow are mostly based on the indicator dilution technique, where an indicator, such as radioisotopes, iodinated agents, dyes, cold saline ect., injected into the blood stream, makes it possible to record changes of indicator concentration in the region or vessel of interest over time (4;5)

Swan-Ganz catheter, used for estimating cardiac output, is based on a thermo dilution method using cold saline as indicator (6). Positron Emission Tomography (PET) and Single Photon Emission Computed Tomography (SPECT) use unstable isotopes in imaging and measure mainly blood flow in the brain (4). Iodinated agents are used as indicators in conventional contrast-enhanced perfusion computed tomography (CT) and can provide both qualitative and quantitative estimates (7). Digital subtractions angiography also uses iodinated agents to enhance the attenuation in vessels, however, the method only provides qualitative information (8). Contrast enhanced magnetic resonance imaging using gadolinium chelates as the indicator agent is used for both imaging and quantifying blood flow. The bolus of contrast creates, in contrast to iodinated agents, a drop in signal intensity in the voxel, which can be related to the blood flow (9).

Electromagnetic flowmeter does not use the indicator dilution principle albeit it is an invasive method for flow measurement. A magnetic field is applied over the vessel of interest. In the vessel, a catheter with two electrodes mounted on the tip is inserted. Knowing the electric and the magnetic field, the blood velocity can be estimated (5).

Non-invasive techniques

Non-invasive techniques for blood flow measurement in vessels can be performed with a number of different techniques: laser Doppler flowmetry, plethysmography, magnetic resonance phase contrast angiography and Doppler ultrasound.

Laser Doppler flowmetry solely measures microcirculation down to 1 mm in the dermis and only as a blood flux in arbitrary perfusion units. Laser Doppler flowmetry is primarily used as an evaluation tool of endothelial function (10). Plethysmography is used for investigation of limb blood flow, yielding a global blood arterial inflow for the investigated limb (11), while the selective evaluation of small vessels, sections of vessels, blood flow in the major vessels and cerebral blood flow are only feasible non-invasively with magnetic resonance angiography and ultrasound Doppler techniques (5).

The techniques used in magnetic resonance for non-invasive blood flow measurements are mainly the time-of-flight and the phase contrast sequences even though a lot of novel sequences are emerging such as blood oxygenation level dependent (BOLD) and arterial spin labeling techniques (12). In this thesis is only used the phase contrast technique, which ECG-triggered can provide quantitative blood flow measurements. The method is accepted as the gold standard for non-invasive cerebral blood flow estimation and has been validated accordingly both *in-vivo* and *in-vitro* (13-18). Phase contrast angiography is a subtraction technique where two images are obtained with different gradients and subtracted from each other (19). The contrast between blood and surrounding tissue is achieved by manipulating the magnetization of moving and stationary spins. The phase of the magnetization from the stationary spin is zero and the phase of the magnetization from the moving spin is non-zero. Thereby, direction and velocity of the moving blood can be derived from the obtained phase velocity maps (20).

The assessment of blood flow with magnetic resonance angiography regardless of the applied sequence is time-consuming, the equipment is expensive and non-mobile, the evaluation is not performed in real time and the estimates are not instantaneous. Conversely, Doppler ultrasound, which is the clinical method of choice for real time assessment of blood velocities is an easily manageable and fast technique, the equipment is mobile, relatively inexpensive, and providing instantaneous estimates. However, the current Doppler systems suffer from several limitations. In this thesis possible solutions are given to some of the limitations: the angle dependency, the relatively low frame rate of the B-mode images and the relatively low temporal resolution in the velocity estimation.

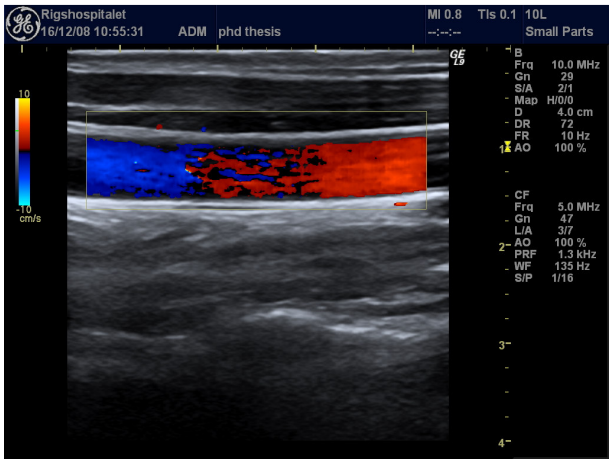

Figure 1
Color flow mapping of the carotid artery is shown. It can only be used for qualitative evaluation. Note that with an angle of insonation of 90°, no velocities are measured.

Doppler ultrasound

In conventional Doppler methods, pulses with 4-8 cycles are emitted at frequencies of 2-15 MHz. The ultrasound, scattered by the moving blood cells, are received by the transducer as echoes and then converted to a voltage signal. On the basis of time-of-flight from emission of the signal to reception of the echo, the position of the moving blood cell can be determined, while the velocity of the motion is found from a measured phase shift (21;22). The velocity estimate is only found along the ultrasound

beam direction, i.e. in the axial direction. Formally, this can be described as,

$$v_z = \frac{f_p c}{2 f_o} \quad (1),$$

where v_z is the axial velocity, f_p is the Doppler frequency, f_0 is the centre frequency of the emitted ultrasound pulse and c is the speed of sound. As transverse flow to the beam direction is not found, the operator is impelled to achieve an acceptable angle of insonation (< 70°) to record the blood motion.

In color flow mapping, no angle correction is performed and thus, no correct velocities are given. Consequently, color flow mapping is only used as a qualitative method for visualizing flow. In Fig. 1, an ultrasound duplex scan image of the common carotid artery is shown.

Angle dependency

In spectral Doppler examination, angle correction is applied on blood velocities estimated within the range gate. The spectral Doppler method is used quantitatively as it is believed that true velocities are displayed after angle correction. This can be seen from the relationship between the axial velocity v_z given by (1) and the true velocity of the blood v given by,

$$v = \frac{v_z}{\cos\theta} = \frac{f_p c}{2 f_o \cos\theta} \quad (2),$$

where θ is the angle between the ultrasound beam and the blood flow. All variables in (2) can be estimated if the operator manually supplies the scanner with the angle θ assuming blood flow parallel to the vessel wall. When performing angle correction in spectral Doppler examination, it is as in color flow mapping compulsory to achieve an angle of insonation below 70°. When the angle approaches 90° reliable velocity estimates cannot be obtained with (2) as cos(90) ~ 0 and small deviations between the angle estimated visually by the operator and the correct angle between blood flow and beam direction result in large errors when calculating the velocity v.

However, not even an acceptable angle of insonation is a guarantee for correct velocity estimation. Tola et al. showed differences of 24-25% for peak systolic and end-diastolic velocities between measurement obtained with fixed angles of 45° and 60° (23) and Hoskins showed an overestimation of maximum velocity by 20% at 50°, 15-30% at 60° and 24-46% at 70° (24).

Not only poses the angle of insonation a problem in the velocity estimation, also the necessary assumption made by the operator concerning the direction of the blood flow is problematic. In the ideal situation, the rigid and straight vessel encompasses a laminar flow parallel to the vessel boundaries, and the angle correction scheme can be made. Vessels are curving and highly elastic creating skewed velocity profiles (25-27) with secondary velocity components (28-32), which makes such an assumption a source of measurement error (33). Thus, it is in general impossible to predict the direction of a blood scatterer based on the B-mode image (24;34-36).

The problem becomes even more evident when examining vessels with complex geometries as the flow profile in these areas always are multidirectional. At bifurcation, branching, valve or any kind of constriction, the pulsative nature of human blood flow will give rise to disturbed or even turbulent flow, where flow direction rapidly changes within the heart cycle. Correcting for the angle would therefore imply that the operator has an a priori knowledge of the direction of the blood scatterers at any location for any image, which clearly is impossible.

In conclusion, an error will always be associated with the conventional Doppler methods with or without angle correction due to angle dependency, and information on the complex flow patterns is kept unrevealed (37;38).

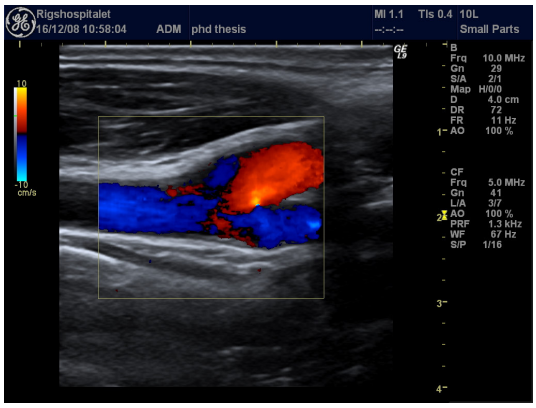

Figure 2
Color flow mapping of the carotid bifurcation is shown. The complex flow patterns are only visualized as a confusing blend of colors.

Accuracy and reproducibility of Doppler ultrasound

Precise information of blood flow is desirable and especially of the blood flow in complex geometries with disturbed flow and vortices as these regions have predilection for atherosclerotic lesions (37-40). The limitation of conventional Doppler ultrasound has been reflected in several papers concerning the validity and reproducibility. Hoskins showed that velocity parameters such as maximum blood velocity, mean blood velocity and volumetric flow had errors of up to 100% depending especially on angle of insonation and blood velocity (41), Krams et al. investigated volume flow estimation assuming parabolic flow and showed 24% error compared to a computational fluid dynamic model (33). However, studies showing the opposite have also been published e.g. Walker et al. using a string phantom reported only up to 5% overestimation of mean velocity (42) and Deane et al. reported 5% error in volume flow estimation with a commercial multigated Doppler system (43). Stewart et al. reported that the color Doppler accuracy was significantly dependent on transducer type, angle of insonation, the actual blood velocity and instrument settings such as pulse repetition frequency and wall filter frequency (44). Also operator and centre dependency have been addressed and several studies actually recommended centre specific validation to normalize for interequipment variation (45-47). Paivansalo et al. carried out an *in-vivo* interobserver and interequipment study and showed variation of up to 61% for equipment and up to 42% variation between observers. In the study it was recommended in addition to centre specific validation, the use of the same operator and equipment for follow-up measurements to reduce the variability of estimates (48). Likewise, Henry-Feugeas et al. explored the variability on the operator and equipment level. While no equipment dependency was found, it was recommended to repeat measurements to reduce a significant operator variability (49).

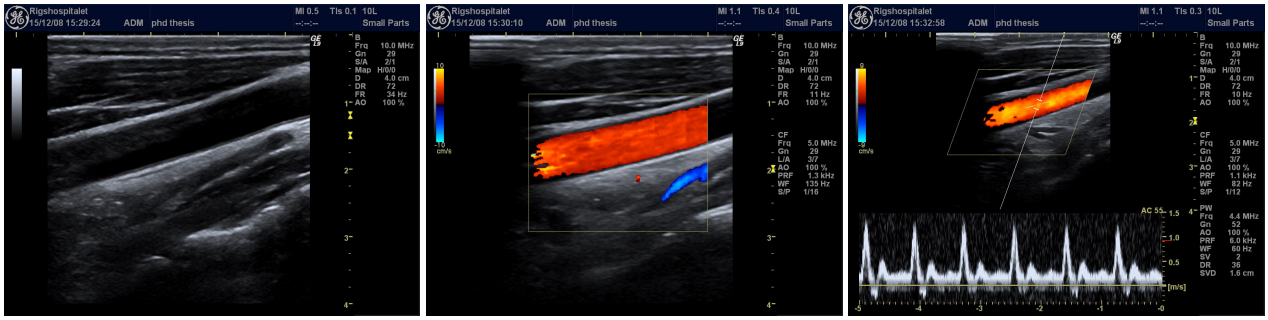

Figure 3
Frame rate decreases from 34 Hz to 10 Hz when adding color flow mapping and spectral Doppler to B-mode imaging. Frame rate on the screen is denoted FR.

Vector velocity imaging

The estimate of blood motion in more than the axial direction is termed a vector velocity (24). Several authors have tried to bypass the angle dependency in conventional Doppler systems and efforts have been made to create such an ultrasound system. Daigle et al. used a multi transducer pulsed Doppler system (50), Fox applied two beams (51), Trahey et al. and Bohs et al. used speckle tracking (52;53), Newhouse et al. used the total bandwidth of the received signal (54), Bonnefous worked with several beamformers in parallel (55), Dunmire et al. proposed a cross-beam technique (56) and Overbeck et al. used an ultrasound unit with a single transmitting and two receiving transducers (57). However, these techniques have neither been evaluated in clinical trials nor have they made it into commercial systems. In this thesis four vector velocity methods all developed at CFU (Center of Fast Ultrasound Imaging) of DTU (Technical University of Denmark) were investigated: Transverse Oscillation, Synthetic Transmit Aperture, Directional Beamforming and Plane Wave Excitation.

Frame rate and temporal resolution

Other limitations in conventional Doppler systems examined in this thesis are frame rate and temporal resolution. Frame rate is mainly governed by the number of pulses used per frame and by the distance each pulse has to travel between transducer and target. It means that scanning depth, pulse repetition frequency and the number of modalities used simultaneously affect frame rate performance (21;58). Also the placement and size of the color box in color flow imaging as well as the placement of the range gate in spectral Doppler dictate the data acquisition time (59). The larger and deeper placed the color box and the deeper placed the range gate, the lower the frame rate will be. B-mode images on high-end scanners are acquired with frame rates up to 50 Hz and can be reduced down to 8-10 Hz in 2-D duplex mode (B-mode combined with color flow mapping), which clearly is unsuitable for visualizing rapid temporal changes in the blood flow as pointed out by Ferrara et al. (60). The problem is aggravated in 2-D triplex mode (B-mode image, color flow mapping and spectral Doppler) and will be a major hurdle in 3-D duplex/triplex scanning.

A typical B-mode frame consists of about 100 image lines where each line is generated from a number of emissions. Whether the technique is color flow mapping, power Doppler or spectral Doppler the axial velocity of blood is found by imaging the same image line repeatedly. In spectral Doppler the estimates are angle corrected by the operator and presented as blood velocities plotted against time denoted a spectrogram (Fig. 3). In most commercial scanners Welch's method is used for estimation of the spectrogram (61) and to obtain an acceptable spectral resolution, a window of up to 256 consecutive emissions is used for each velocity estimate (58).

The temporal resolution of the conventional spectrogram can be impaired to the point where the rapid changes of blood velocities in the systole are difficult to measure. The events of upstroke, peak velocity and downstroke lie temporally so close that the different phases are merged together due to the long observation window (62). Furthermore, the frame rate of the interleaved B-mode images can be decreased to the point where the examination is difficult to perform (58;60). The operator can experience difficulties in placing the range gate in the vessel of interest. The reasons are often respiratory movement by the patient or involuntary transducer movements by the operator, which are not realized and corrected as the B-mode image used for navigation is not updated adequately.

The problem of inadequate processing power especially in 2-D triplex scan mode is in several commercial scanners solved by reducing triplex to a pseudo-triplex scan mode. All three modalities are present on the working screen ex. B-mode image, color flow mapping and spectral Doppler but only two modalities are running simultaneously, thus, reducing the computational demands. On the commercial scanner, which generated the frames shown in Fig. 3, triplex mode is implemented as such.

In different experimental setups and by several groups, the limitations in frame rate and temporal resolution have been tried solved. Coats et al. used offline computation combined with a recursive spectral estimation approach (62), Tanaka et al. used selected phase information (63), Udesen et al. proposed a method with chirp excitation signal and frequency splitting (64), Gran et al. proposed a similar method but with Barker and Golay code excitation signal (65), Oddershede et al. used multi-frequency encoding (66) and Jensen used sparse data sequences (67). Also adaptive filtering have previously been tried by Li et al. (68), Herment et al. (69) and Vaikus et al. (70;71). In this thesis two approaches for high frame rate/temporal resolution are investigated: Plane Wave Excitation and adaptive filtering on spectral velocity data using the BAPES and BPC approaches.

AIMS OF STUDIES

Study I and II concerned angle independent ultrasound vector velocity techniques. Stroke volume measurements were obtained *in-vivo* with three different experimental vector velocity ultrasound techniques: Transverse Oscillation, Synthetic Aperture Transmit and Directional Beamforming, and compared to magnetic resonance imaging using phase contrast angiography. The aims of the studies were to validate *in-vivo* the ultrasound vector

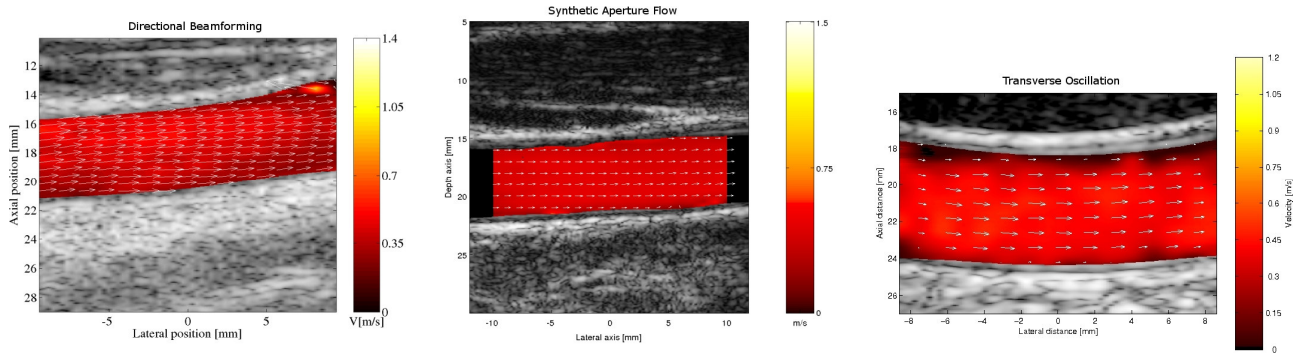

Figure 4

Frames obtained with Directional Beamforming, Synthetic Transmit Aperture and Transverse Oscillation are shown. The frames are recorded from different volunteers and to different time. The vector arrows, superimposed onto color flow maps, delineate magnitude and direction of the moving blood scatterers.

velocity methods to magnetic resonance angiography in terms of measured stroke volume.

Study III concerned yet another angle independent ultrasound vector velocity technique called Plane Wave Excitation that can obtain vector velocity estimates with a high frame rate. The aim of the *in-vivo* study was to investigate flow patterns in complex geometries of the human cardiovascular system in healthy volunteers and compare the results to the literature.

Study IV focused on the two adaptive spectral estimators BAPES and BPC. The estimators can generate spectrograms using shortened observation windows, which results in spectrograms with a high temporal resolution. The aim of the study was to validate quantitatively and qualitatively BAPES and BPC *in-vivo* against the conventional method for spectral estimation.

MATERIALS, METHODS AND RESULTS

The studies were all performed after approval by The Danish National Committee on Biomedical Research Ethics (Date: 30-05-6, J.nr:(KF)07307579).

In study I and II, the same eleven healthy volunteers (seven males and four females, 24 – 44 y, mean age: 32 y) were included after informed consent. The right common carotid artery was examined in all volunteers using ultrasound and magnetic resonance angiography. The volunteer rested supine on the examination table 15 min prior to all examinations.

In study III, four healthy volunteers (three males and one female, 26 – 45 y, mean age: 34 y) were included after informed consent. Complex vessel geometries were scanned in supine or standing position depending on scan location.

In study IV, ten healthy volunteers (nine males and one female, 24-36 y, mean age: 29 y) were included after informed consent. The right common carotid artery was examined in all volunteers using ultrasound.

All scans whether ultrasound or magnetic resonance angiography in the studies were carried out by KLH. All the *in-vivo* results obtained with the experimental methods were recorded with the experimental scanner RASMUS (1;2) and post-processed using MATLAB (Mathworks, Natick, MA, USA) on a 100 CPU Linux cluster. This combination gave a very flexible and unique environment for emitting, receiving and processing signals from an experimental point of view, but the processing time was considerable for all methods. It took seconds to acquire the data, hours to store and up to two full days to process. Obviously, this affected the logistics and reduced the number of samples that realistically could be enrolled into the study populations.

Table 1

Overview of volunteers included in to the four studies

	study I	study II	study III	study IV
no. of volunteers	11	11	4	10
mean age	32	32	34	29
male/female	7/4	7/4	3/1	9/1
experimental method(s)	TO	TO/STA/DB	PWE	BAPES/BPC
reference method	MRA	MRA	none	Welch's method

Transverse Oscillation method

The Transverse Oscillation method has been proposed by Jensen and Munk (72;73) and evaluated in simulations, in flow rig and *in-vivo* by Udesen et al. (36;74). The Transverse Oscillation method tracks scatterer motion along two orthogonal axes by emitting a conventional Doppler pulse. The velocity component in the axial direction is found exactly as in conventional Doppler ultrasound. An oscillation in the transverse direction is created by changing sensitivity of the receiving elements and the velocity along the transverse direction is found from the frequency content of this oscillation. By combining the velocity component along the two axes, vector velocities are achieved.

Directional Beamforming method

The Directional Beamforming method has been proposed by Jensen and Bjerngaard (75;76), evaluated in simulations (77;78) and examined in flow rig and *in-vivo* by Holfort et al. (79). In Directional Beamforming a focused pulse is emitted with the focal point placed below the depth of interest. Hence, the acoustic energy around the scatterer is sufficient for beamforming echo lines in a star-shaped pattern with the scatterer of interest as the centre. Lines are compared through a normalized cross-correlation across matching angles for consecutive pulses (80). The highest normalized cross-correlation is ideally found for the correct angle. When the correct angle is known, the magnitude of the motion along the correct echo line is found through cross-correlation for consecutive pulses.

Synthetic Transmit Aperture method

The Synthetic Transmit Aperture method has been proposed by Jensen and Nikolov (81) and evaluated in simulations, in flow rig and *in-vivo* (82-85). A Synthetic Transmit Aperture image is acquired by emitting a spherical unfocused wave from a few elements and receiving the scattered signal with all elements. Since the position for the emission is known, the precise origin of the received scattered signal can be calculated from time-of-flight for all elements and used in focusing. The Synthetic Transmit Aperture approach generates one low-resolution image for every

emitted pulse. A high-resolution image is constructed by adding a number of consecutive low-resolution images. For every emission, a high-resolution image can be created by applying a recursive approach, where the oldest transmission event is replaced by the newest. The Synthetic Transmit Aperture method can therefore yield a frame rate equal to pulse repetition frequency with focus in all image points.

An approach to estimate vector velocities, identical to Directional Beamforming is computed. Echo lines in a star-shaped pattern are created to every point of interest and compared between emission-identical high-resolution images for every angle. The normalized cross-correlation peaks for the right angle. The magnitude is found through cross-correlation across echo-lines of the right angle for consecutive pulses.

Plane Wave Excitation method

The Plane Wave Excitation method has been proposed by Udesen et al., and simulations, flow rig and *in-vivo* evaluations have been reported (86;87). In Plane Wave Excitation all elements of the transducer are excited at the same time thereby creating a pressure wave with a nearly plane front. The unfocused pulse covers the entire imaging plane with acoustic energy and a full speckle image is obtained for every emission. To increase the penetration of the signal into the tissue, a 13 bit Barker code is used instead of a conventional pulse (65). The angle independent vector velocity estimates are found when tracking speckle motion between consecutive speckle images by using a speckle tracking approach called sum of squared differences (52;88). The frame rate of the vector velocity images obtained with Plane Wave Excitation in study III was 100 Hz. However, matching receive and transmit channels in RASMUS would give a frame rate of 200 Hz without degrading the quality of the vector velocity estimates.

Blood spectral Power Capon method

The BPC method has been proposed by Stoica et al. (61;89), evaluated in simulations by Jensen et al. (77;78), and in flow rig and *in-vivo* by Gran et al. (90). The BPC method is a spectral estimator using adaptive filtration on data. Unique filters are designed to every velocity component in the data set. Hence, a unique matched filterbank is generated for each specific data set where the total power of the filters for each velocity of interest is minimized while not distorting the signal of interest.

Blood Amplitude and Phase Estimation method

The BAPES method has been proposed by Gran et al. (91) and evaluated in simulations by Jensen et al. (77;78), and in flow rig and *in-vivo* by Gran et al. (90). The BAPES method is based on a matched filterbank framework as BPC (61;92). However, in the BAPES method the filtered noise power is minimized fulfilling the constraint that the signal of interest is not distorted.

Previous simulations and phantom studies carried out by Gran et al. (90) have indicated that the two adaptive methods BPC and BAPES can obtain spectrograms with sufficient spectral resolution and contrast using fewer data than the conventional method for spectral Doppler estimation.

Magnetic resonance angiography

In study I and II, magnetic resonance angiography was used as the reference method. The examinations were performed with a 1.5 Tesla whole body scanner (Magnetom Vision, Siemens AG). A prospective ECG triggered phase contrast sequence using a cervical coil was employed. (Phase interval: 29 ms, echo time: 7 ms, flip angle: 30°, FOV: 100 mm, slice thickness: 6 mm, VENC: ±1.5 m/s, pixel resolution: 0.52 x 0.39 mm^2 in a matrix of 192 x 256 pixels interpolated up to 256 x 256 pixels).

Welch's method

In study IV, the Welch's method was used as the reference method. Two different weighting schemes were applied on data, which resulted in different performances: Welch's method with a Hanning window (W.HAN) and Welch's method with a boxcar window (W.BOX). According to the basic principles in digital processing (93), W.HAN has a good contrast at the expense of spectral resolution, while W.BOX has a good spectral resolution at the expense of contrast. W.HAN is the preferred conventional spectral estimator.

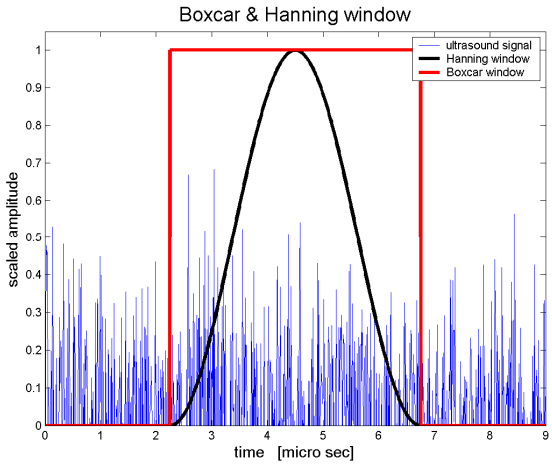

Figure 5
The scattered signal is multiplied in the time domain with a bell-shaped Hanning window or with a rectangular boxcar window. Thus, the blood signal used for velocity estimation is found under the curve corresponding to the chosen window.

Study I:

In-vivo validation of a blood vector velocity estimator with MR angiography (Hansen KL, Udesen J, Thomsen C, Jensen JA, Nielsen MB. In Vivo Validation of a Blood Vector Velocity Estimator with MR Angiography. IEEE Trans Ultrason Ferroelec Freq Contr 2009;56:91-100)

Study I concerned *in-vivo* validation of the angle independent ultrasound vector velocity technique Transverse Oscillation. Stroke volume measurements of the common carotid artery were obtained *in-vivo* on 11 healthy volunteers and compared to measurements obtained with magnetic resonance imaging using phase contrast angiography.

The Transverse Oscillation measurements were performed with angles of insonation of approximately 90°, i.e. when the conventional Doppler method fails to estimate any blood velocities, and the vessel of interest was scanned approximately two cm upstream of the bifurcation to prevent confounding complex flow. For each vector velocity image, the vessel region was automatically identified from the B-mode image by an algorithm described by Udesen et al. (36). The volume flow per second in each vector velocity image was estimated by integrating the delineated 2-D vessel up to form a 3-D vessel. The mean volume flow per second in each vector velocity image was found as an average of the volume flows per second estimated to all different lateral positions in the vector velocity image. This yielded a volume profile for every sequence. A detailed description of the calculations is given by Hansen et al. (27).

The volume flow obtained with magnetic resonance angiography was found in the scan plan perpendicular to the right common carotid artery and two cm upstream of the bifurcation as with the Transverse Oscillation method. For each velocity map an anatomic image was calculated. A threshold pixel value defined the region of interest on the anatomic images in order to discriminate between the pixel values of blood and vessel boundaries. The region of interest encompassing the lumen of the vessel was used as a window on the phase velocity maps to ensure that velocity values from the vessel surroundings representing e.g. the jugular vein was ignored in the volume flow measurement. A region near the common carotid artery was selected to correct the phase off-set (94). The volume flow to each frame was found by multiplying the velocity with the area it occupied i.e. the pixel area and then adding up all the pixel derived volume flows encompassing the region of interest. The volume flow profile was given by the estimated volume flows of the full sequence of frames.

Assumption

To investigate the assumptions of circular geometry and rotationally symmetric blood flow necessary for computing stroke volume from the vector velocity estimates obtained with Transverse Oscillation, an additional approach was carried out. The assumptions were tested by taking out lines from the phase velocity maps to every angle. The lines of velocity values were treated as if they were obtained with Transverse Oscillation, i.e. in the longitudinal scan plane. Thus, for every angle the 1-D line taken from the phase velocity map was integrated up to form a 2-D circle resulting in a volume flow estimate. For every volunteer a stroke volume range encompassing the stroke volume variation over all angles was found. This was compared to the actual magnetic resonance angiography stroke volume measurement where the velocities of the entire region of interest were used and no assumptions were made.

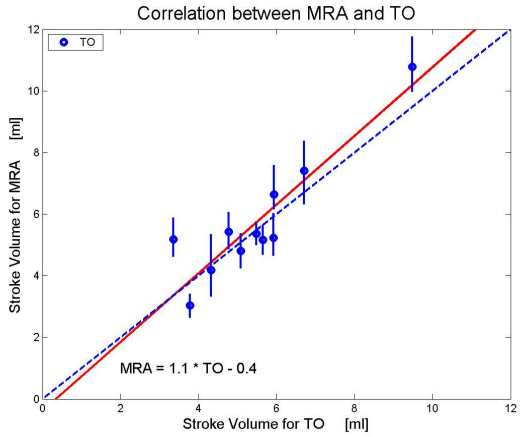

Figure 6
Correlation between magnetic resonance angiography and Transverse Oscillation. Line of best fit (solid line) and line of perfect fit (dashed line) are drawn. The range of magnetic resonance angiography stroke volume assuming circular geometry and rotationally symmetric flow is shown for every volunteer as a bar.

Statistics

A descriptive statistical analysis was computed on the stroke volume data for the two modalities finding mean value, standard deviation and stroke volume range. The stroke volume data obtained with Transverse Oscillation was then compared to stroke volume data obtained with magnetic resonance angiography using linear regression analysis with two-tailed significance value given and $p<0.05$ considered significant. The correlation coefficient, regression equation, and confidence interval using Fisher's r-to-z-transformation were calculated. Finally a Bland-Altman plot was made to illustrate the difference of stroke volume estimated by Transverse Oscillation and magnetic resonance angiography. Statistical analyses were performed using SAS (SAS Institute, Cary, NC, USA) and MATLAB (Mathworks, Natick, MA, USA).

Results

The mean stroke volume ± one standard deviation for Transverse Oscillation was 5.5 ml ± 1.7 ml with the range of 3.4 – 9.5 ml. Respective estimates for magnetic resonance angiography were 5.8 ml ± 2.0 ml with the range 3.0 – 10.8 ml.

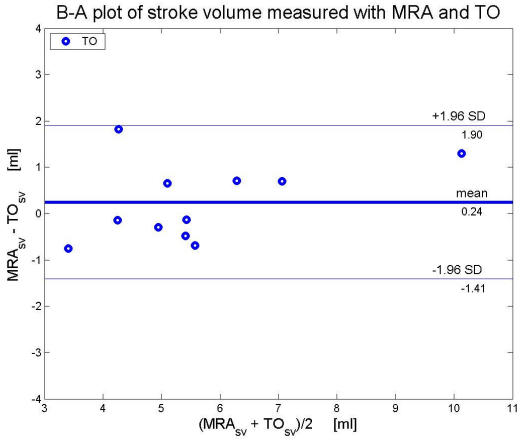

Figure 7
Bland-Altman plot of stroke volume measured with magnetic resonance angiography and Transverse Oscillation showing mean (thick solid line) ± 1.96 standard deviations (thin solid line).

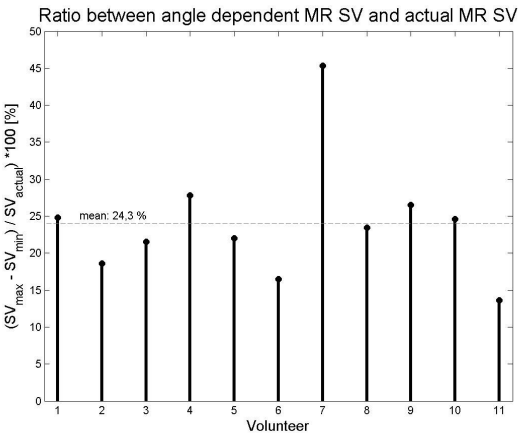

Figure 8
Stroke volume ratio was estimated by the range, found as the difference between the maximal and minimal angle dependent stroke volume, divided with the actual magnetic resonance angiography stroke volume and given in percentage. The mean ratio was 24.3 %.

The correlation between the stroke volume estimated by Transverse Oscillation and magnetic resonance angiography is illustrated in Fig. 6 as a scatterplot. *R* was 0.91 ($p<0.01$; 95 % confidence interval: 0.69 to 0.98) and the least squares (MRA = 1.1 * TO - 0.4) was found to be close to unity. The range of magnetic resonance angiography stroke volume assuming rotationally symmetric flow and circular vessel geometry is shown as a bar for every volunteer in the scatterplot. In Fig. 7, the Bland-Altman plot

is constructed. The mean difference is 0.24 ml with limits of agreement at -1.41 ml and 1.90 ml (95% confidence interval for mean difference: -0.32 ml to 0.81 ml). In Fig. 8, the stroke volume range as percentages of the actual magnetic resonance angiography stroke volume is plotted for all volunteers, giving a mean ratio of 24.3%. One volunteer (no. 7) presented a ratio between the magnetic resonance angiography stroke volume range and the actual magnetic resonance angiography stroke volume of 48.3%. The angle dependent stroke volume with a range of 3.2 ml to 5.1 ml for this volunteer is depicted in Fig. 9. By examining the phase velocity maps of this particular volunteer, it was seen that a substantially asymmetric flow was present, while the vessel had an approximately circular geometry.

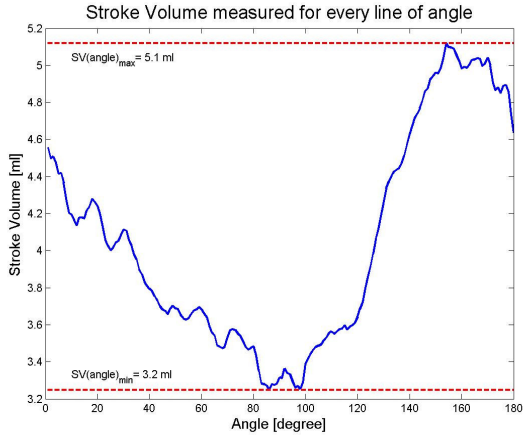

Figure 9
Stroke volume measured for every line of angle for one volunteer. The maximal and minimal angle dependent stroke volume estimates are shown as dashed lines.

In conclusion, volume flow measurements were obtained *in-vivo* with the angle independent blood vector velocity method Transverse Oscillation. The results validated against volume flow measurements obtained with magnetic resonance angiography were found to be comparable for stroke volume using correlation, regression and Bland-Altman analyses. With Transverse Oscillation a method has been introduced to obtain quantitative blood flow measurements from the entire frame.

Study II:

In-vivo comparison of three ultrasound vector velocity techniques to MR phase contrast angiography (Hansen KL, Udesen J, Oddershede N, Henze L, Thomsen C, Jensen JA, Nielsen MB. In vivo comparison of three ultrasound vector velocity techniques to MR phase contrast angiography. Ultrasonics 2009;49:659-667)

In this study, Directional Beamforming, Synthetic Transmit Aperture and Transverse Oscillation were validated against magnetic resonance angiography in a setup similar to study I. Stroke volume measurements of the common carotid artery were obtained *in-vivo* on 11 healthy volunteers and compared to measurements obtained with magnetic resonance phase contrast angiography. Transverse Oscillation was included to compare the performances between the three vector velocity ultrasound methods. The ultrasound measurements were performed with angels of insonation of approximately 90° and two cm upstream of the bifurcation. The volume flow estimates deriving from measurements of the three vector velocity methods were calculated in an approach similar to the approach described in study I. The magnetic resonance angiography data was identical to the data used in study I and was treated accordingly. Also the statistics were identical to study I using descriptive statistical and linear regression analyses as well as Bland-Altman plots.

Results

The stroke volume in the right common carotid artery was measured for the 11 volunteers with the three ultrasound methods and magnetic resonance angiography. The results are displayed in Table 2 along with mean, standard deviation and range for each modality.

In Fig. 10, the scatter plots are given showing the correlation between the each of the three ultrasound techniques and magnetic resonance angiography, with Directional Beamforming vs. magnetic resonance angiography: R=0.84 (p<0.01, 95% confidence interval: 0.49 to 0.96); Synthetic Transmit Aperture vs. magnetic resonance angiography: R=0.71 (p<0.05, 95% confidence interval: 0.19 to 0.92) and Transverse Oscillation vs. magnetic resonance angiography: R=0.91 (p<0.01, 95% confidence interval: 0.69 to 0.98). No significant differences were observed for any of the three comparisons (Directional Beamforming vs. magnetic resonance angiography: p=0.65; Synthetic Transmit Aperture vs. magnetic resonance angiography: p=0.24; Transverse Oscillation vs. magnetic resonance angiography: p=0.36). The

Table 2
Stroke volume measurements recorded in study II. For all volunteers, mean stroke volume ± one standard deviation and stroke volume range were obtained with Directional Beamforming, Synthetic Transmit Aperture, Transverse Oscillation and magnetic resonance angiography.

Volunteer no.	DB [ml/heart beat]	STA [ml/heart beat]	TO [ml/heart beat]	MRA [ml/heart beat]
Volunteer 1	4.81	5.58	3.78	3.03
Volunteer 2	5.02	7.45	5.65	5.17
Volunteer 3	6.48	6.95	5.93	6.64
Volunteer 4	9.31	6.74	6.71	7.41
Volunteer 5	6.00	5.83	4.78	5.43
Volunteer 6	9.53	9.70	9.48	10.78
Volunteer 7	3.92	4.16	4.32	4.18
Volunteer 8	3.66	4.24	5.09	4.80
Volunteer 9	4.08	8.50	5.92	5.23
Volunteer 10	3.72	5.25	3.36	5.18
Volunteer 11	4.85	4.89	5.49	5.36
mean SV +/- SD	5.58 +/- 2.10	6.30 +/- 1.76	5.30 +/- 1.65	5.75 +/- 2.02
range	3.72 - 9.53	4.16 - 9.70	3.36 - 9.48	3.03 - 10.78

resultant Bland-Altman plots are shown in Fig. 11. The mean difference, with confidence interval and limits of agreement are given for all plots in Table 3. The confidence interval for the mean differences overlapped zero for all three methods and was narrowest for Transverse Oscillation and broadest for Synthetic Transmit Aperture (Transverse Oscillation: 1.13 ml; Directional Beamforming: 1.56 ml; Synthetic Transmit Aperture: 1.97 ml). This also applied to the limits of agreement (Transverse Oscillation: 3.31 ml; Directional Beamforming: 4.55 ml; Synthetic Transmit Aperture: 5.74 ml). In terms of mean differences in the Bland-Altman plots, Directional Beamforming was the most precise method followed by Transverse Oscillation and Synthetic Transmit Aperture (Directional Beamforming: 0.17 ml; Transverse Oscillation: 0.24 ml; Synthetic Transmit Aperture: -0.55 ml).

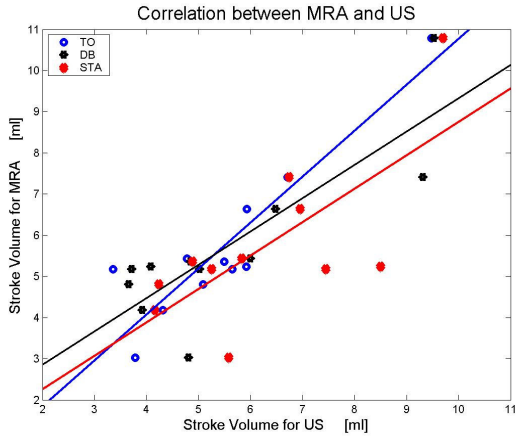

Figure 10
Graph showing the correlation between magnetic resonance angiography and the three ultrasound methods. The line of best fit is drawn for each comparison.

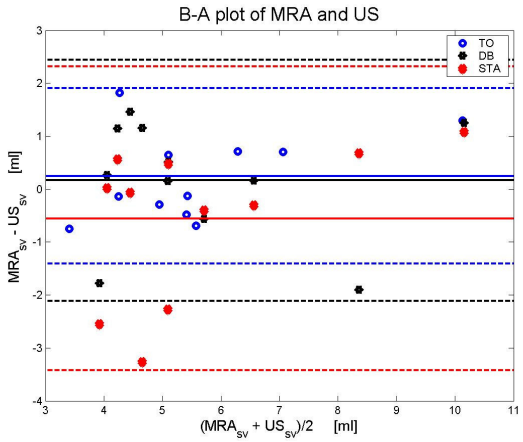

Figure 11
Bland-Altman plots of stroke volume measurements comparing magnetic resonance angiography with each of the three ultrasound methods showing mean ± 2 standard deviations as solid and dashed lines, respectively.

Table 3
Mean of difference with confidence interval, upper and lower limits of agreement given for the Bland-Altman plots.

Method	Mean [ml] (95% CI)	Lower limit [ml]	Upper limit [ml]
DB vs. MRA	0.17 (-0.61 to 0.95)	-2.11	2.44
STA vs. MRA	-0.55 (-1.54 to 0.43)	-3.42	2.32
TO vs. MRA	0.24 (-0.32 to 0.81)	-1.41	1.90

In conclusion, study II showed that it was possible to obtain reliable quantitative measurements *in-vivo* with the three different angle-independent 2-D vector velocity methods, Directional Beamforming, Synthetic Transmit Aperture, and Transverse Oscillation when compared to magnetic resonance angiography.

Study III:

In-vivo examples of flow patterns with the fast vector velocity ultrasound method (Hansen KL, Udesen J, Gran F, Jensen JA, Nielsen MB. In-vivo Examples of Flow Patterns With The Fast Vector Velocity Ultrasound Method. Ultraschall in Med. 2009;30(5):471-77)

In study III, different vessel locations were examined with the Plane Wave Excitation method. Four healthy volunteers with no history of cardiovascular disease were scanned on locations with complex vessel geometries encompassing multidirectional blood motion. Scan sequences were acquired of two carotid bifurcations, two femoral bifurcations, the bifurcation at the brachiocephalic trunk, the bifurcation of the subclavian artery as well as the internal jugular vein and the great saphenous vein, both with venous valves. The scans were all recorded with the volunteers in supine position except the scan of the great saphenous vein, where the volunteer was in standing position while performing dorsal and plantar flexion to simulate walking.

In Fig. 12, the vortex formation in the carotid bulb of two different volunteers is shown. In the left frame the internal carotid artery is seen as the superficial vessel while in the right frame it is seen as the deep vessel. For both volunteers a vortex with low velocities in the carotid bulb was present during the entire heart cycle. Apart from the vortical recirculation in the bulb no retrograde flow was present.

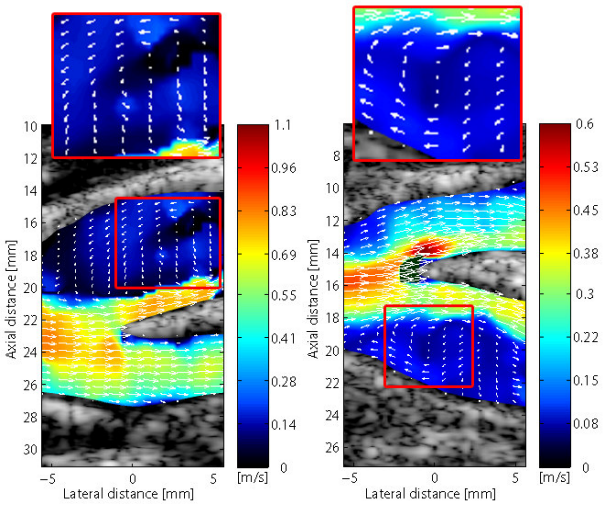

Figure 12
In the bulb of the internal carotid artery a vortex was present during the entire heart cycle. The depicted frames were both taken from systole.

In Fig. 13, the brachiocephalic trunk is shown. No vortex was present in systole but disturbed flow was seen in the subclavian artery when flow reversed at end-systole and end-diastole. In diastole the flow was filling the common carotid artery (superficial vessel) from the subclavian artery (deep vessel). Thus, the diastolic flow was retrograde in the subclavian artery and antegrade in the common carotid artery.

The same volunteer was scanned on the right side bifurcation of the thyrocervical trunk and the vertebral artery. Two frames are shown in Fig. 14. During peak systole the flow propagated without disturbed flow from the subclavian artery to the vertebral artery (superficial vessel) and the thyrocervical trunk

(deep vessel) as seen in the left frame. Vortices in the subclavian artery scanned in the cross-sectional plane were visible right after peak systole and throughout diastole (right frame). The secondary flow swept from the superficial part of the subclavian artery and downwards in an s-shaped pattern creating two vortices.

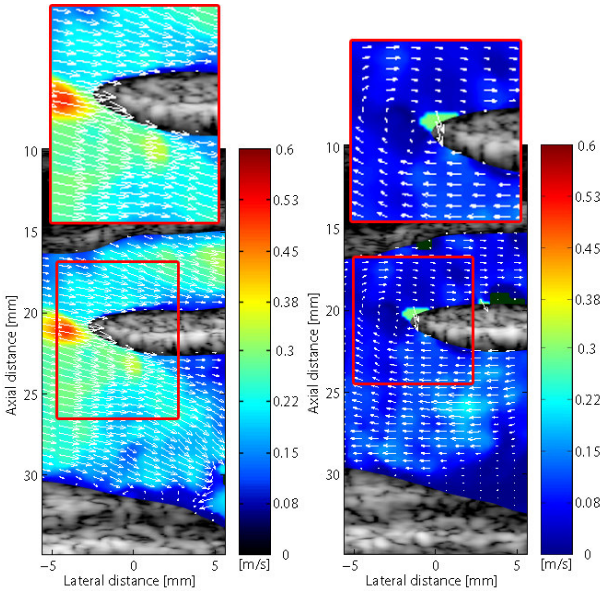

Figure 13
No vortex was seen in the brachiocephalic trunk during systole (left frame). The diastolic flow was going from the subclavian artery (deep vessel) to the common carotid artery (superficial vessel) (right frame).

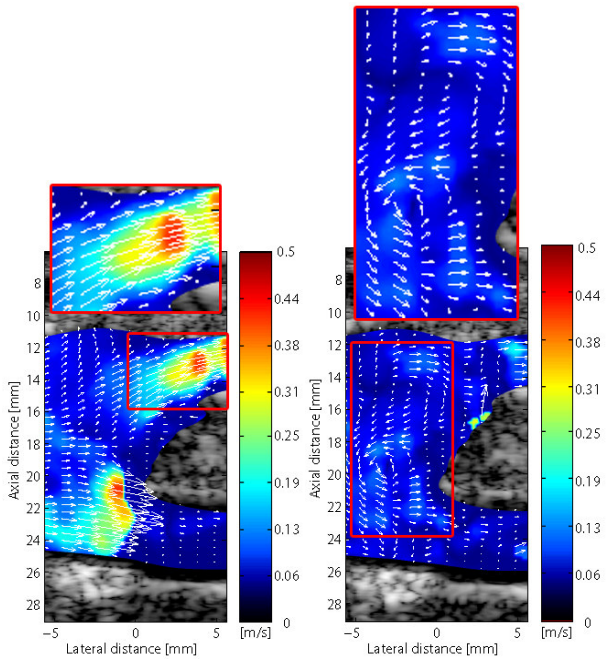

Figure 14
No disturbed flow in the vertebral artery (superficial vessel) and the thyrocervical trunk (deep vessel) was present during peak systole (left frame). In the subclavian artery vortices were present after peak systole and throughout diastole. The frame is taken from the beginning of diastole (right frame).

In Fig. 15, frames of two femoral bifurcations taken from examinations on two different volunteers are shown. Laminar flow was seen during the entire heart cycle with reversed flow in the superficial branch in the beginning of diastole.

The venous valves of the great saphenous vein and internal jugular vein were scanned. In Fig. 16, a venous bulb of the saphenous vein is depicted. Although the valves were not visible, the effect of the valves on the flow was obvious. During opening of the valves the flow was squeezed to form a jet. Furthermore, vortices were formed in the pockets behind the valves. No retrograde flow was present and during the closed phase bidirectional blood motion was seen with the competent valves as a separator.

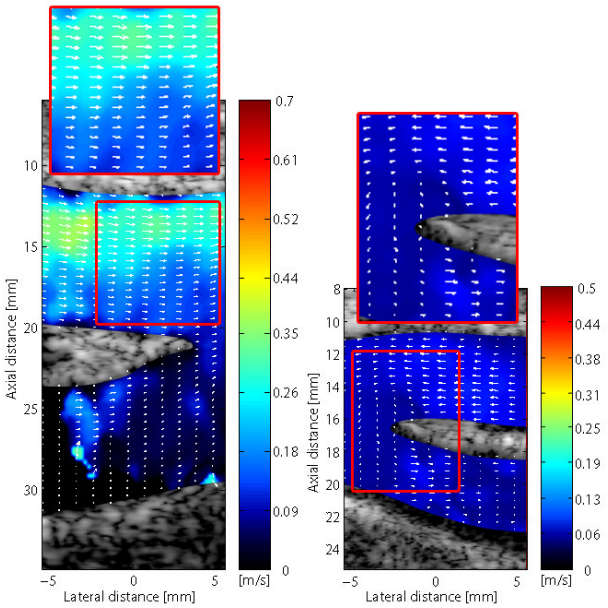

Figure 15
During diastole reversed flow in the superficial branches of the femoral arteries for two volunteers were present.

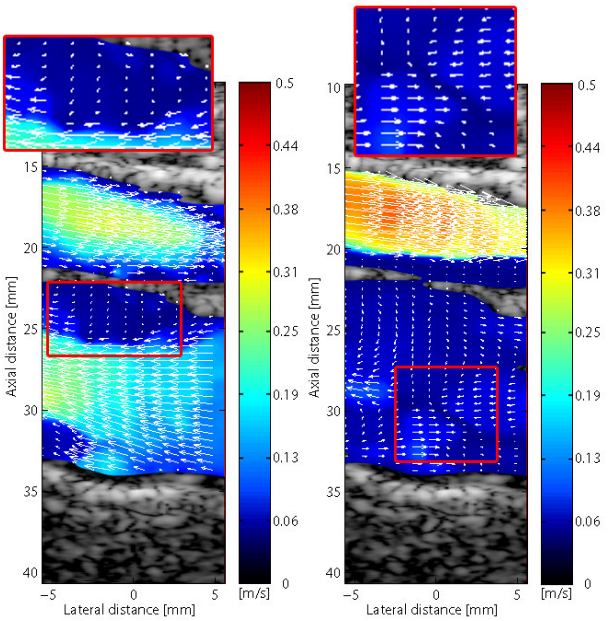

Figure 16
In the great saphenous vein (deep vessel) a jet was formed during antegrade flow between the valves, and vortices were formed behind the valves (left frame). The valves were competent and no retrograde flow was present (right frame). The femoral artery is seen as the superficial vessel in both frames.

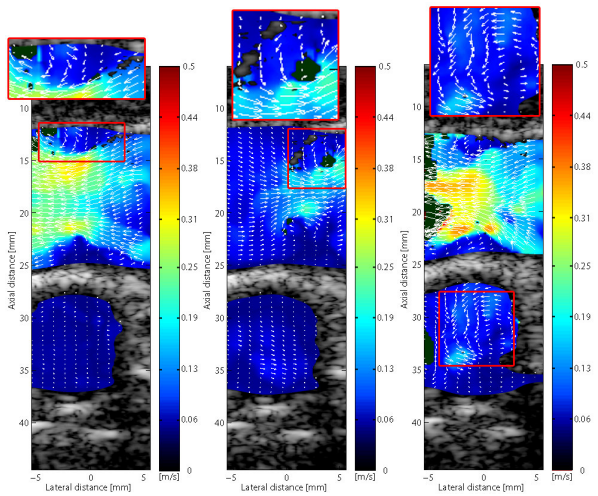

Figure 17
In the jugular vein (superficial vessel) the flow was squeezed by incompetent venous valves forming a jet during antegrade and retrograde flow (left and middle frame, respectively). Vortices were formed in the pockets behind the valves during antegrade flow and upstream of the valves during retrograde flow. In the carotid artery (deep vessel) secondary flow was seen during systole when scanned in the short axis (right frame).

The valves of the jugular vein are visible in Fig. 17. The flow pattern around the valves was similar to the flow pattern observed in the great saphenous vein except that retrograde flow was observed due to incompetent valves. Vortices were formed in the pockets behind the valves and a jet was formed between the valves during the opened phase (left frame). During retrograde flow a jet was formed between the valves with vortices upstream of the valves (middle frame). The common carotid artery was scanned in the cross-sectional plane, and a secondary flow was observed during systole (right frame).

In conclusion, study III showed that the Plane Wave Excitation method can visualize complex flow patterns with a high frame rate. The results indicate that novel information on fluid dynamics can be achieved with Plane Wave Excitation and may in the future be a tool for cardiovascular disease assessment. Even though widespread anatomic variations of the arterial as well as the venous system dictate individual flow patterns not to be generalized, the results obtained with Plane Wave Excitation are glimpses of a far more complex blood dynamics than previously reported. Table 4 provides an overview of the findings with data given on gender, age and scan location.

Table 4
Overview of the findings in study III with data given on gender, age and location.

Volunteer no.	Gender	Age	Location	Findings
Volunteer 1	male	34	carotid bifurcation	stable vortex in the bulb
-	-	-	femoral bifurcation	retrograde flow in the superficial branch, antegrade flow in the deep branch
-	-	-	femoral vein	vortices in the pockets, competent valves
Volunteer 2	female	45	carotid bifurcation	stable vortex in the bulb
Volunteer 3	male	26	jugular vein	vortices down- and upstream of the incompetent valves, secondary flow in the carotid artery
-	-	-	brachiocephalic trunk	retrograde flow in the subclavian artery, antegrade flow in the carotid artery
-	-	-	subclavian bifurcation	S-shaped secondary flow in the subclavian artery
Volunteer 4	male	31	femoral bifurcation	retrograde flow in the superficial branch, antegrade flow in the deep branch

Study IV:

In-vivo validation of fast spectral velocity estimation techniques

(Hansen KL, Gran F, Pedersen MM, Holfort IK, Jensen JA, Nielsen MB. In-vivo validation of fast spectral velocity estimation techniques. Ultrasonics 2010;50:52-59)

In study IV, adaptive filtering in spectral Doppler was investigated and compared to conventional algorithms for spectral Doppler estimation. Ten healthy volunteers were scanned on the right common carotid artery. One data set was recorded for each volunteer and post processed using the four different methods: W.HAN, W.BOX, BPC and BAPES. For each method, spectrograms were estimated using different observation windows (OW): 128, 64, 32, 16, 8, 4 and 2 emissions/estimate. Thus, from every data set, were calculated 28 spectrograms giving in total 280 spectrograms for all volunteers.

To investigate the methods quantitatively, a spectrum corresponding to end-diastole was found for each spectrogram. For each data set, the time instant was chosen by visually examining the spectrogram obtained with W.HAN at OW 128. To the chosen time, spectra to all 28 spectrograms of the same data set were found. End-diastole was chosen to be the time of interest as it is easy to indentify and used clinically for calculating resistive index and systolic-diastolic ratio (95). From each spectrum, two parameters were calculated: the Full-Width-at-Half-Maximum (FWHM) and the ratio between main and side lobe levels. The FWHM was found as the width of the velocity distribution of the main lobe at half of the maximum amplitude. Thus, the FWHM given in m/s is a measure of spectral resolution. The ratio was found as the relative difference between the side-lobe level and the peak amplitude. The side-lobe level was found as the median value of the distributed amplitudes outside the main-lobe, outlined by the FWHM. The ratio, given in decibel (dB), is a measure of contrast in the spectrogram.

To investigate the methods qualitatively, nine experienced radiologists evaluated in a blinded trial the 280 randomized spectrograms by scoring each spectrogram useful or not useful. Intra- and interobserver variations were additionally found. The intraobserver variability was assessed by comparing the scores given twice by three radiologists with >14 days between each session. The sequence of spectrograms was randomized to each session so judgment bias was minimized.

Statistics

A descriptive statistical analysis was computed on FWHM and ratio estimates of the 280 spectra finding mean value and standard deviation for each combination of method and window. The

Table 5
Mean (and standard deviation) of FWHM and ratio given for each combination OW/method over ten volunteers

OW	Parameter	BAPES	BPC	W.HAN	W.BOX
128	FWHM [m/s]	0.029 (0.01)	0.026 (0.01)	0.034 (0.01)	0.029 (0.01)
	ratio [dB]	37.06 (3.19)	33.64 (3.16)	34.47 (3.20)	32.80 (2.45)
64	FWHM [m/s]	0.025 (0.01)	0.032 (0.01)	0.050 (0.01)	0.040 (0.01)
	ratio [dB]	35.81 (3.91)	29.89 (2.76)	31.53 (2.63)	29.31 (1.87)
32	FWHM [m/s]	0.034 (0.02)	0.033 (0.02)	0.074 (0.01)	0.055 (0.01)
	ratio [dB]	34.02 (4.47)	28.71 (2.94)	30.67 (4.63)	26.60 (2.25)
16	FWHM [m/s]	0.029 (0.01)	0.027 (0.01)	0.124 (0.00)	0.082 (0.01)
	ratio [dB]	33.27 (5.24)	29.03 (4.41)	29.63 (5.81)	22.99 (1.73)
8	FWHM [m/s]	0.034 (0.01)	0.033 (0.02)	0.230 (0.00)	0.159 (0.01)
	ratio [dB]	31.26 (5.17)	26.01 (4.18)	26.49 (5.33)	17.85 (0.81)
4	FWHM [m/s]	0.065 (0.02)	0.053 (0.03)	0.412 (0.01)	0.319 (0.00)
	ratio [dB]	26.73 (4.73)	22.23 (4.01)	20.51 (3.29)	13.20 (0.60)
2	FWHM [m/s]	0.145 (0.03)	0.113 (0.06)	0.688 (0.01)	0.688 (0.01)
	ratio [dB]	23.38 (4.13)	18.94 (4.18)	11.21 (0.51)	11.21 (0.51)

scores given by the radiologists were pooled by method and window. Useful and not useful were coded with the dummy variables 1 and 0, respectively. Before data analysis, Kolmogorov-Smirnov normality test and the Levene variance homogeneity test were applied to the data. No data transformation was needed. Bonferroni adjusted tests for multiple comparisons paired on volunteer level with $p<0.05$ considered significant were performed (96). The intra- and interobserver variability were investigated using Cohen's and Fleiss' kappa, respectively (97;98). Statistical analyses were performed using SAS (SAS Institute, Cary, NC, USA) and MATLAB (Mathworks, Natick, MA, USA).

Results

From a data set of one volunteer with three systoles recorded, examples of spectrograms generated with the four methods at OW 128 and 16 are presented in Fig. 18. The gaps in the spectrograms represent the necessary pulse emissions used for generating the interleaved B-mode images.

Examples of spectra obtained at end-diastole to time 2.2 s from the spectrograms shown in Fig. 18 are presented in Fig. 19. Mean and standard deviation of FWHM and ratio for the 280 spectra pooled by method and window are displayed in Table 5 and plotted in Fig. 20. The overall result of the scores given for each combination of method and window is displayed in Table 6 and illustrated in Fig. 21. The result of the Bonferroni adjusted tests for multiple comparisons paired on volunteer level is shown in Table 7 and illustrated in Fig. 22.

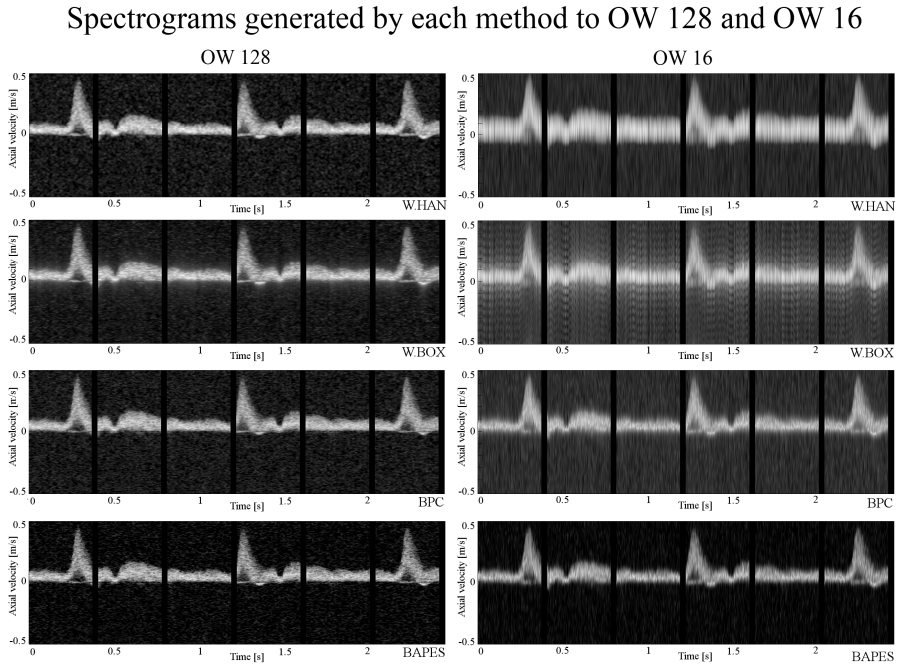

Figure 18
Spectrograms were found using the four methods with an OW 128 (left frames) and 16 (right frames). At OW 128 all methods displayed good performances. At OW 16, W.HAN and W.BOX estimated spectrograms with decreased quality compared to BPC and BAPES.

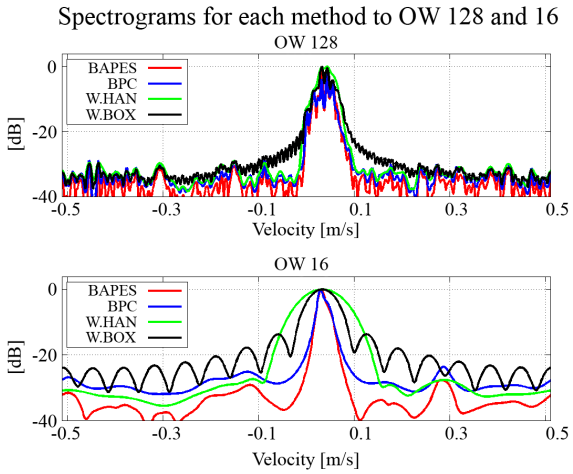

Figure 19
From the same volunteer at one time instant, spectra were generated using the four methods with an OW 128 and 16.

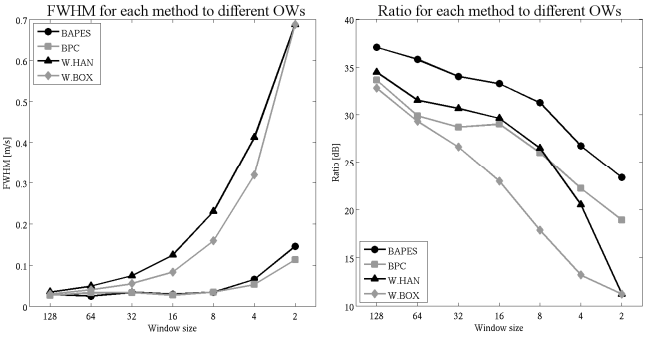

Figure 20
FWHM (left frame) and ratio (right frame) are plotted against OW for each method.

Table 6
Each cell consists of the total sum of scores given by nine radiologists on 10 volunteers in the range 0 to 90 (and percentage) for the combination method/OW.

OW	BAPES	BPC	W.HAN	W.BOX
128	72 (80 %)	73 (81.1 %)	73 (81.1 %)	62 (68.9 %)
64	73 (81.1 %)	78 (86.7 %)	75 (83.3 %)	55 (61.1 %)
32	80 (88.9 %)	77 (85.6 %)	34 (37.8 %)	23 (25.6 %)
16	70 (77.8 %)	50 (55.6 %)	5 (5.6 %)	5 (5.6 %)
8	31 (34.4 %)	13 (14.4 %)	0 (0.0 %)	0 (0.0 %)
4	6 (6.7 %)	6 (6.7 %)	0 (0.0 %)	0 (0.0 %)
2	0 (0.0 %)	0 (0.0 %)	0 (0.0 %)	0 (0.0 %)

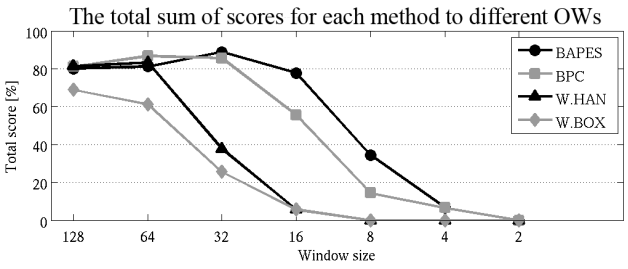

Figure 21
The total sum of scores in percentage for each method to different OWs

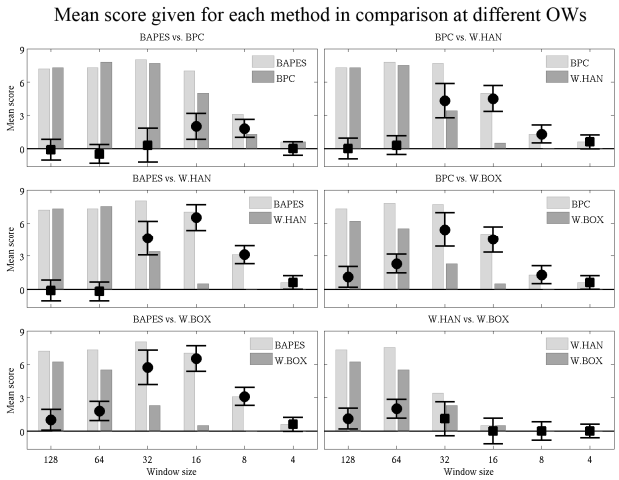

Figure 22
The mean score is with a histogram and the 95% confidence interval for the difference in means as a bar (■=insignificant and ●=significant).

For each method, tests for multiple comparisons were also used to investigate at which OWs the given scores were significantly different from the scores given at OW 128. W.BOX performed significantly worse when OW was reduced to 64 compared to W.BOX at OW 128 (p=0.03). W.HAN was not scored differently when reducing OW to 64 (p=0.55) but was scored significantly less at OW 32 (p<0.0001). BPC performed equally well at OW 32 compared to OW 128 (p=0.30) while BAPES scored significantly higher at OW 32 compared to OW 128 (p=0.02). Only BAPES performed as well for OW 16 as at OW 128 (p= 0.55). All four methods had decreased performances at OW 8, 4 and 2 compared to OW 128. The intraobserver variability for three radiologist evaluating the same 280 spectrograms with >14 days apart showed good agreement with an averaged Cohen's kappa value of 0.79 (94%, κ=0.88; 83%, κ=0.67; 93%, κ=0.81). The interobserver variability showed moderate agreement using Fleiss' kappa (78%, κ=0.57).

In conclusion, study IV showed that the adaptive methods were superior to the conventional Welch's method and that BAPES was superior to BPC.

The quantitative tests showed that BAPES and BPC had improved spectral resolution and BAPES had improved spectral contrast compared to Welch's method. According to the given judgments, OW can be reduced to 32 when using BPC, and 16 when using BAPES method for estimating spectrogram without losing performance. The results indicate that the adaptive methods BPC and BAPES potentially can bring improvements to spectral blood estimation as an increase of the temporal resolution of the spectrogram or as an increase of the frame rate for the interleaved B-mode images.

DISCUSSION

New achievements

No previous studies have validated vector velocity or adaptive spectral estimators *in-vivo*, and no previous studies have obtained *in-vivo* sequences of angle independent instantaneous vector velocity images at a frame rate of 100 Hz. In study I and II, it was shown that experimental vector velocity methods can produce reliable stroke volume measurements *in-vivo* when compared to magnetic resonance phase contrast angiography. In study III, it was shown that a vector velocity method acquiring estimates at a

Table 7
The mean of scores is given on volunteer level in the range 0 to 9 (and standard deviation) for each combination method/OW. Each comparison test between methods indicated by "x" is given with 95% CI in difference of means and p-value (●=significant).

	BAPES	BPC	W.HAN	W.BOX	95% CI	p-value
128 emissions/estimate	7.2 (0.91)	7.3 (0.65)	7.3 (0.95)	6.2 (1.23)		
BAPES vs. BPC	x	x			(-1.03;0.83)	1.0
BAPES vs. W.HAN	x		x		(-1.03;0.83)	1.0
BAPES vs. W.BOX	x			x	(0.07;1.93)	0.03 ●
BPC vs. W.HAN		x	x		(-0.93;0.93)	1.0
BPC vs. W.BOX		x		x	(0.17;2.03)	0.01 ●
W.HAN vs. W.BOX			x	x	(0.17;2.03)	0.01 ●
64 emissions/estimate	7.3 (0.82)	7.8 (0.79)	7.5 (0.97)	5.5 (0.71)		
BAPES vs. BPC	x	x			(-1.34;0.35)	0.63
BAPES vs. W.HAN	x		x		(-1.04;0.64)	1.0
BAPES vs. W.BOX	x			x	(0.95;2.65)	<0.0001 ●
BPC vs. W.HAN		x	x		(-0.54;1.15)	1.0
BPC vs. W.BOX		x		x	(1.45;3.15)	<0.0001 ●
W.HAN vs. W.BOX			x	x	(1.15;2.85)	<0.0001 ●
32 emissions/estimate	8.0 (0.94)	7.7 (1.25)	3.4 (1.51)	2.3 (1.25)		
BAPES vs. BPC	x	x			(-1.24;1.84)	1.0
BAPES vs. W.HAN	x		x		(3.06;6.14)	<0.0001 ●
BAPES vs. W.BOX	x			x	(4.16;7.24)	<0.0001 ●
BPC vs. W.HAN		x	x		(2.76;5.84)	<0.0001 ●
BPC vs. W.BOX		x		x	(3.86;6.94)	<0.0001 ●
W.HAN vs. W.BOX			x	x	(-0.44;2.64)	0.31
16 emissions/estimate	7.0 (1.15)	5.0 (1.15)	0.5 (0.53)	0.5 (0.53)		
BAPES vs. BPC	x	x			(0.84;3.16)	0.0002 ●
BAPES vs. W.HAN	x		x		(5.34;7.66)	<0.0001 ●
BAPES vs. W.BOX	x			x	(5.34;7.66)	<0.0001 ●
BPC vs. W.HAN		x	x		(3.34;5.66)	<0.0001 ●
BPC vs. W.BOX		x		x	(3.34;5.66)	<0.0001 ●
W.HAN vs. W.BOX			x	x	(-1.16;1.16)	1.0
8 emissions/estimate	3.1 (1.10)	1.3 (0.94)	0 (0)	0 (0)		
BAPES vs. BPC	x	x			(0.99;2.61)	<0.0001 ●
BAPES vs. W.HAN	x		x		(2.29;3.91)	<0.0001 ●
BAPES vs. W.BOX	x			x	(2.29;3.91)	<0.0001 ●
BPC vs. W.HAN		x	x		(0.49;2.11)	0.0006 ●
BPC vs. W.BOX		x		x	(0.49;2.11)	0.0006 ●
W.HAN vs. W.BOX			x	x	(-0.81;0.81)	1.0
4 emissions/estimate	0.6 (0.84)	0.6 (0.70)	0 (0)	0 (0)		
BAPES vs. BPC	x	x			(-0.62;0.62)	1.0
BAPES vs. W.HAN	x		x		(-0.02;1.21)	0.062
BAPES vs. W.BOX	x			x	(-0.02;1.21)	0.062
BPC vs. W.HAN		x	x		(-0.02;1.21)	0.062
BPC vs. W.BOX		x		x	(-0.02;1.21)	0.062
W.HAN vs. W.BOX			x	x	(-0.62;0.62)	1.0
2 emissions/estimate	0 (0)	0(0)	0(0)	0(0)		

high frame rate can reveal novel information of complex blood flow *in-vivo*. Finally, it was shown in study IV that spectrograms can be produced *in-vivo* with adaptive spectral methods and that these experimental methods outperform the conventional spectral estimator.

Previous studies

Experimental ultrasound methods for volumetric measurements have previously been examined by other groups. Kim et al. validated cardiac output estimates obtained *in-vivo* with a 2-D ultrasound system using color Doppler mapping of the short axis view, which showed good agreement compared with both

thermo dilution (-0.16 ±0.94 l/min) and magnetic resonance (0.21 ±0.83 l/min)(99). Kripfgans et al. obtained in a flow phantom, volume flow measurements in the same manner but extended to a 3-D ultrasound system where the measured volume flow rates were within ±15% of actual values (100). An *in-vivo* validation study of volumetric flow obtained by an invasive Doppler flow wire system was published by Jenni et al. where excellent correlation was found compared to transit-time flowmeter (R=0.97) (101) and Krams et al. reported on an experimental multigated spectral Doppler system validated in a flow phantom with an error less than 15% compared to computational fluid models (33). Two studies have reported on a technique based on multigated dual-ultrasound beam technology and it was shown that reliable volume flow in flow phantoms and *in-vivo* could be obtained when compared to conventional spectral Doppler (102;103). Shuping et al. and Forsberg et al., both validated 4-D Doppler ultrasound systems for volumetric flow *in-vivo*. Shuping et al. compared the estimates to phase contrast MRA with good agreement (R=0.92) and Forsberg et al. compared the volumetric estimates to a transit-time flowmeter also showing good agreement (R^2=0.86 for mean volume flow and R^2=0.62 for maximum volume flow) (104;105). It should be noted that none of the mentioned studies of experimental ultrasound methods for volumetric measurements were done with actual angle independent methods as all the experimental methods were based on conventional Doppler.

Studies of accuracy and reproducibility of experimental ultrasound methods with reduced angle dependency have also been carried out. Schank et al. examined a triangulation method for blood flow estimation in a flow phantom and *in-vivo* by repositioning the transducer using a position locating system. The phantom experiment revealed 5% error for velocity magnitudes and error of less than 3° in Doppler angle when the angle of insonation was kept below 75° (106). Steel et al. reported maximum velocity variation of 7.6% for insonation angles between 40° to 80° obtained in a phantom study using a dual-beam ultrasound method on a split aperture system (107) and extended later this to an *in-vivo* study for inter- and intraobserver variation (intraobserver: -41.3 to 45.2 cm/s; interobserver:-29.6 to 46.8 cm/s) (108). Likewise, Ricci et al. reported on accuracy and reproducibility for a dual-beam system based on two separate transducers. The phantom experiment showed a mean error of velocity magnitude of 1.9%, the reproducibility tests showed a variation of 0.8% to 10% on the estimates and the *in-vivo* experiment showed intraobserver variation of ±9.6% (109). Though the methods have reduced angle dependency they still have impaired performances at angles close to 90° and cannot visualize complex flow.

Angle independent methods for visualizing blood flow have also been examined. Fei et al. estimated velocities in the carotid artery and bifurcation with an approach where blood velocities were reconstructed from three different scan sessions of varying insonation angles. The estimates compared to conventional spectral Doppler estimation agreed well (R=0.94) (34;110). However, the method cannot provide instantaneous vector velocities as several cardiac cycles are used for each velocity estimation. Nyrnes et al. examined an approach called Blood Flow Imaging where speckle motion is visualized. In a setup similar to study IV, the usefulness was examined in comparison to conventional color Doppler imaging when scanning arterial septal defect *in-vivo*. The study indicated that the technique improves the visualization of interatrial blood flow in children (111). Also Lovstakken et al. reported on the technique in a study concerning intraoperative assessment on blood flow patterns in coronary anastomoses (112). It should be noted that the speckle imaging technique visualizes flow with a high frame rate but without any quantitative parameters. Pastorelli et al. reported on multigated dual-beam method. Real-time angle independent vector velocity maps were validated in a flow phantom with velocity magnitude error of 23% and examples of *in-vivo* measurements were shown. The method performs with a frame rate of 6 Hz and down to a maximal scanning depth of 1 cm due to the necessary beam crossing (113).

Reference modalities

In study I and II, three vector velocity methods were validated *in-vivo* through volumetric flow measurements. In *in-vivo* setup no control of the flow is possible, which gives emphasis to the need of a reliable reference method. No reference can measure instantaneous velocity estimates to all points in the scan plane. Spectral Doppler ultrasound only interrogates the velocity distribution along a single line and several studies have shown the inaccuracy both in respect to estimated blood velocities and volumetric flow estimation (114). Magnetic resonance phase contrast angiography measures velocity estimates as an average over several heart cycles covering the entire lumen of the vessel in through-plane setup. The accuracy, reproducibility and interobserver variability of magnetic resonance phase contrast angiography have been assessed in numerous studies and the method has been reported to be both accurate and robust (115-118). As a consequence, magnetic resonance phase contrast angiography is accepted as the gold standard for non-invasive, cerebral blood flow estimation (13-17) and was therefore chosen to be reference method in study I and II.

RASMUS (1;2) is not magnetic resonance compatible (as most other ultrasound systems) and therefore, the scans were performed at different examinations. This affected the alignment of scan planes in the rotational and longitudinal direction, and the point-to-point comparison of the estimates, as the velocity profile fluctuates over time. Therefore, the comparison of the vector velocity estimates was made with respect to volume flow and more specifically stroke volume as this variable is less heart rate dependent and thus, a more reliable parameter when comparing volumetric measurements obtained at two different occasions (119).

In magnetic resonance angiography the blood flow is measured in a plane perpendicular to the longitudinal axis of the vessel using a through-plane encoding. Intuitively, it would have been a better comparison to choose an end-plane setup aligned with the two encoded directions of the corresponding vector velocity measurement to examine each voxel in pairs. Apart from difficulty of scan plane alignment, the inadequate in-plane resolution (slice thickness) in magnetic resonance angiography of 6 mm would confound the blood signal with the vessel surroundings and result in underestimated velocities. Furthermore, it has been shown that flow measurements acquired with a through-plane flow encoding are more precise than those acquired with end-plane flow encoding (118).

In study IV, the reference modality was the conventional method for spectral Doppler estimation called Welch's method. The method was applied with two different window settings so both reference spectrograms with good contrast and good spectral resolution were used in the comparison with BPC and BAPES. As each acquired data set was processed by all four methods, a direct comparison was feasible and no considerations of bias as a consequence of time or acquisition differences are necessary.

Assumption of rotationally symmetric flow and circular vessel geometry

In 2-D ultrasound vector velocity estimation, out-of-plane velocity data is not acquired and only a single projection through the long axis of the vessel is examined. On the contrary, the data obtained with phase contrast angiography in through-plane flow encoding covers the entire short axis, i.e. lumen of the vessel. To reduce the information gap between the two methods in compare, a simple *in-vivo* model, was chosen. The normal common carotid artery is a straight vessel with an expected unidirectional flow and is parallel to skin surface (120;121). Moreover, the vessel is assumed to have a circular geometry and an expected symmetric flow profile.

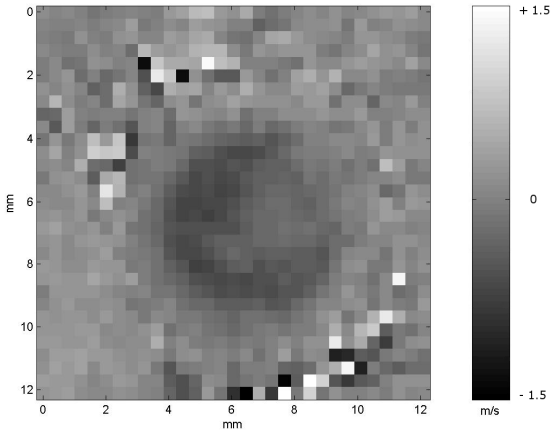

Figure 23
Phase velocity map of the common carotid artery of one volunteer taken from late systole showing marked asymmetry of the flow profile.

The assumptions necessary for the vector velocity derived stroke volume calculations were investigated for all 11 volunteers. 1-D lines from the phase velocity maps to every angle were integrated up to form 2-D circles from which stroke volume estimates were derived. There showed to be a remarkable difference in stroke volume estimates over all 180 degrees with a mean of 24.1% for the examined volunteers (Fig. 8). It underlines that the assumption of circular geometry and rotationally symmetric flow profile is a simplification. By examining the different magnetic resonance phase velocity maps, it was evident that the asymmetric flow profile contributed most to the angle dependent stroke volume difference. In Fig. 23, a phase velocity map of the common carotid artery of one volunteer is shown. The phase velocity map is taken from late systole and visualizes the marked asymmetry of the flow profile. This is consistent with Brands et al. and Tortoli el al., whom both reported asymmetry of the flow profile in the common carotid artery of healthy volunteers (25) and especially after the systolic peak (122).

Thus, the placement of the longitudinal scan plane through the centre axis of the vessel in the ultrasound examination was an important confounder to study I and II. According to the magnetic resonance angiography data, the stroke volume obtained with the vector velocity methods could change up to 24.3% simply by changing the insonation window of the same vessel section.

Additionally, misplacement of the ultrasound planes away from the centre axis would add up to the bias. When performing the ultrasound examination it was crucial to scan the vessel parallel to the longitudinal axis exactly through the centre axis where the diameter of the lumen was largest, and where intima was most clearly delineated. Vessel intima was a reliable marker when positioning the scan plane through the middle of the vessel, because the layer structures were most clearly visible when the ultrasound beam direction was perpendicular to the planes of the layers. However, vessels are not perfectly straight tubes and inevitably a part of the centre axis will be out of the scan plane due to curvature resulting in underestimation of the averaged volume flows.

Clutter filtering

The echo signal of moving blood is about 100 times weaker than the echo signal deriving from soft tissue (60;123). One of the major challenges in 2-D ultrasound velocity estimation is clutter filtering, where stationary echoes from the vessel surroundings, i.e. soft tissue, are cancelled out (124). Clutter filtering was one of the most important confounders in study I and II as blood signal representing low velocities near the vessel wall was cancelled out together with clutter signal.

The Transverse Oscillation method is the most robust method in terms of echo cancelling as a result of the lateral oscillation and the estimates in study I and II obtained with this method were done with only one filter applied. Synthetic Transmit Aperture

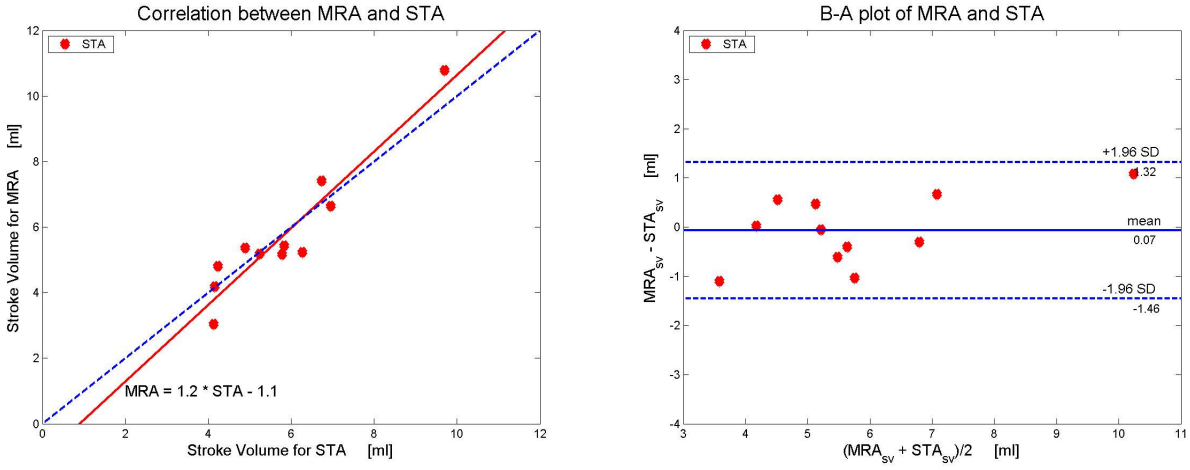

Figure 24
When applying a second filter for the three outliers a correlation plot is given for which $R = 0.95$ ($p<0.01$; 95% confidence interval: 0.82 to 0.99) and a Bland-Altman plot with a mean difference of -0.07 ml (95% confidence interval: -0.54 ml to 0.41 ml) and limits of agreement from -1.46 to 1.32 ml.

and Directional Beamforming use the same scheme for velocity estimation. Nevertheless, the Synthetic Transmit Aperture method potentially has an advantage in terms of echo cancelling as the method uses continued data that can be echo cancelled with very long filters.

This was not reflected in the results (Table 3, Fig. 10 and Fig. 11) as only one filter was used in Synthetic Transmit Aperture while an adaptive filter approach was used in Directional Beamforming. The adaptive filter in Directional Beamforming consisted of two different filters, one for systolic flow and one diastolic flow used for all volunteers. It was employed by manually setting a threshold value for each volunteer defining systole and diastole.

The Synthetic Transmit Aperture measurement deviated from the magnetic resonance angiography measurement for three volunteers: no.1, no.2 and no. 9 (Table 2). When inspecting the vector velocity images it was clear that vector velocities near the vessel wall for the three volunteers were measured inaccurately: in wrong directions and with overestimated magnitudes. The three volunteers acted as outliers presumably as a consequence of a non-moving carotid artery during systole. The filter used in Synthetic Transmit Aperture was optimized to vessel movement as this was present for the majority of the samples. Thus, the mismatch in filter and vessel movement resulted in the observed overestimation of stroke volume for the three outliers. When applying another filter optimized to the reduced vessel movements of the three outliers, an improved overall result appeared for Synthetic Transmit Aperture when compared to magnetic resonance (Fig. 24).

Averaging in magnetic resonance angiography

The volume flow profile consisting of one complete heart cycle was found as a mean of measurements over 192 heart cycles in study I and II, and each data acquisition was triggered by the *R*-peak of the ECG-signal. To ensure that one complete heart cycle was recorded, the data acquisition extended into the second systole. It has previously been addressed that due to fluctuations in heart rate and changing *R*-*R* interval over the averaged heart cycles, the second averaged systole will not be in phase, making it difficult to determine the correct duration of the complete heart cycle (118). In study I and II, the shortest heartbeat of the 192 heart cycles defined the length of the complete averaged heart cycle, i.e. where the upstroke of the second systole initiated. Hence, it is expected that the calculated magnetic resonance angiography stroke volumes were slightly underestimated.

Complex flow patterns visualized in a high frame rate setting

In study III, the vector velocity method Plane Wave Excitation was used to visualize complex flow profiles in the cardiovascular system in both simple and complex vessel geometries. This was carried out to investigate the possibilities of vector flow imaging but also in the attempt to gather new information of fluid dynamics. In total six bifurcations and two veins were examined on four healthy volunteers.

It was shown when examining the carotid bifurcations on two volunteers that a well-defined vortex was present in the carotid bulb during the entire heart cycle (Fig. 12). This is in accordance with earlier results obtained with ultrasound vector velocity examinations (36;125). No stable vortices were observed during systole in the other four bifurcations.

Previous studies with ultrasound Doppler and magnetic resonance imaging have shown retrograde flow in femoral arteries and the brachiocephalic trunk during diastole (106). Study III is consistent with this literature. The new information obtained with Plane Wave Excitation is how the flow reverses. It was shown that the flow in the femoral artery only reversed in the superficial branch while remaining antegrade in the deep branch (Fig. 15) and that the flow in the brachiocephalic trunk reversed in the subclavian artery and remained antegrade in the common carotid artery (Fig. 13).

It is well known that the flow in the carotid arteries is without retrograde flow (126) and it is believed that the antegrade flow in diastole primarily is forwarded from the aorta, denoted the windkessel effect (127). The effect describes how half of the left ventricular stroke volume during systole is stored in the aorta and due to the elastic forces of the aortic wall is forwarded in diastole to the peripheral circulation. The vector velocity sequence obtained with Plane Wave Excitation indicates that the blood reserve forwarded in diastole to the brain could derive from other arteries than the aorta.

It was shown by using Plane Wave Excitation that competent valves in the great saphenous vein were present, and that vortices were formed in the pockets behind valves (Fig. 16). This is consistent with previous studies (128;129). The internal jugular vein was also examined and the examination revealed the presence of incompetent valves and retrograde flow (Fig. 17). Incompetent valves of the internal jugular vein have been described before with prevalence of 36.8% to 38.4% in healthy persons (130-132). The findings concerning flow around valves in the great saphenous vein and the internal jugular vein obtained with Plane Wave Excitation are consistent with the literature. However, vortices on both sides of the valves created by bidirectional flow have not been reported previously.

Finally, secondary flow was seen in the common carotid artery (Fig. 17) and in the subclavian artery (Fig. 14). Secondary flow in different vessels has been predicted by computational fluid dynamics and magnetic resonance imaging in several studies but not before has it been possible to visualize secondary flow with ultrasound (29-32). The secondary flow is thought to have a protective role in the development of atherosclerosis and may be an important issue in vascular disease assessment (133).

The stable vortex of the carotid bulb and its relationship with baroreceptor controlled blood pressure regulation

The vortex is fundamental in the carotid bifurcation and has in numerous studies been linked to the development of atherosclerosis (31;134-136) as disturbed flow around vessel bifurcation has been linked more widely to atheroma deposition (137;138). The findings in study III indicate that flow patterns in the carotid bifurcation are different from flow patterns in other bifurcations of the human cardiovascular system. It appears that the stable vortex is related to the bulb and not the bifurcation. In the bulb, a high concentration of blood pressure regulating baroreceptors is present, and it is therefore reasonably to speculate if the vortex of the carotid bulb is essential in blood pressure regulation (139;140). Bernoulli's principle relates velocity and pressure,

$$\text{Const} = P + \tfrac{1}{2}\rho v^2 \qquad (3),$$

where P is the pressure, ρ is the density of blood, and v the velocity along a flow line. The increase in vessel diameter in the carotid bulb results in a loss of blood velocity, which is counterbalanced by an increase in blood pressure. The carotid bulb can be perceived as a blood pressure amplifier creating high pressure values by slow moving vortices. Hence, the vortices are providing the necessary input for the baroreceptors of the carotid bulb in order to achieve a correct autonomic control of the blood pressure by

the regulating centre in the medulla oblongata. Several authors have previously addressed Bernoulli's principle in relation to bifurcations and venous valves (129;135;141;142), and Henze showed by calculating the pressure gradients from vector velocity estimates that indeed high pressure gradients exist in the carotid bulb during peak systole (143). However, the relationship between the stable vortex, the geometry of the carotid bulb and blood pressure regulation has not previously been addressed nor investigated.

Temporal resolution

In study IV, adaptive spectral Doppler estimators with improved temporal resolution performances were investigated. While the Plane Wave Excitation method achieves a high frame rate performance by manipulating the emitted signal, the adaptive spectral estimators achieve improved performances by using adaptive filtration on the received signal so fewer data is necessary per estimate.

Several groups have proposed adaptive filtering techniques for blood velocity estimation and for the majority of works only simulations have been performed (144;145). Only a few studies have been extended to flow phantom validation and only Herment et al. has produced an example of adaptive spectral filtration on *in-vivo* data (69;146;147). Thus, study IV is unique as an *in-vivo* validation study of adaptive filtering methods for blood velocity estimation. The performances of BAPES and BPC were investigated quantitatively through the parameters FWHM and ratio, and qualitatively by letting radiologists score the resulting spectrograms.

FWHM given in m/s is a measure of spectral resolution and should be as low as possible, while the ratio given in dB is a measure of spectral contrast and should be as high as possible. It is seen in Table 5 and Fig. 20 that on average for all OWs above 2, W.BOX performed with better resolution than W.HAN and W.HAN performed with better contrast than W.BOX. The adaptive methods outperformed Welch's method in terms of resolution at all OWs below 128 and it is seen that BPC had a slightly better resolution than BAPES. In terms of contrast, BAPES was superior compared to both BPC and Welch's method for all OWs. W.HAN had better contrast than BPC for all OWs above 8.

In Fig. 18, examples of acquired spectrograms obtained with the four approaches at OW 128 and 16 are shown. Spectral resolution in the spectrogram corresponds to the width of the white curve representing estimated blood velocities, while the difference between the white curve and the dark surroundings corresponds to contrast. The spectrograms underline the results of the quantitative evaluations. At OW 128 the four approaches produced spectrograms of good quality while the estimators differed in performance at OW 16. At OW 16, it is seen that W.BOX estimated with a higher spectral resolution than W.HAN and the adaptive methods with higher spectral resolution than Welch's method. Furthermore, it is seen that the contrast decreased from BAPES to BPC and Welch's method. W.BOX performed poorest among the four methods in terms of contrast and a so-called ringing phenomenon at OW 16 can be seen.

Spectra for the methods are shown in Fig. 19. The side lobes representing leakage from the true velocity were suppressed, while the main lobe representing the true velocity was broadened for W.HAN compared to W.BOX. The pronounced side lobes for W.BOX at OW 16 correspond to the ringing phenomenon shown in Fig. 18. The adaptive methods had a narrower main lobe at OW 16 compared to Welch's method and BAPES displayed better side lobe levels compared to both BPC and Welch's method.

The overall result of the qualitative evaluation displayed in Table 6 and Fig. 21 shows that the radiologists preferred the adaptive methods over Welch's method, BAPES over BPC and W.HAN over W.BOX. The inter- and intra-observer variability were additionally tested and showed moderate and good agreement, respectively, indicating consistent scores given by each radiologist with a base-line difference among the radiologists. In Table 7 and Fig. 22 the results of the statistical analyses on the mean of scores using Bonferroni adjusted tests for multiple comparisons are displayed. It is seen that at OW 128 and 64, BAPES, BPC and W.HAN performed equally well while W.BOX scored significantly less. When reducing the OW to 32, the adaptive methods BAPES and BPC performed better than W.HAN and W.BOX. However, BAPES was superior to BPC at OW 16 and 8. According to the radiologists, at OW 16 and 8 the conventional methods failed and at OW 4 and 2, all four methods failed.

For each method, the scores given at window sizes below OW 128 were compared to the score given at OW 128 to evaluate how robust each method was to reduction of OW. At OW 64 only W.BOX scored significantly worse, while W.HAN significantly decreased in score at OW 32. At OW 32, BPC scored as at OW 128 while BAPES actually scored significantly better. At OW 16, only BAPES was scored equal to OW 128. Hence, W.HAN at OW 64, BPC at 32 and BAPES at 16 can produce spectrograms, according to the nine radiologists, which are as acceptable as if they were produced at OW 128.

Moreover, the radiologists preferred contrast to spectral resolution when comparing scores given for W.BOX and W.HAN at OW 128 and 64. In most modern scanners the Hanning weighting scheme is accordingly implemented for spectral blood estimation. However, when comparing BPC and W.HAN the improved resolution in BPC was preferred to the improved contrast in W.HAN. This is seen in Table 7 and Fig. 22 at OW 32 and 16. It indicates that it is not only the raised side lobe level in W.BOX, which reduces the quality of the spectrogram compared to W.HAN but also the accompanying ringing phenomenon.

Finally, the radiologists significantly preferred BAPES at OW 32 compared to BAPES at OW 128 (p = 0.01). The reason could be that the observers were disturbed visually by the high contrast and spectral resolution of the spectrograms obtained with BAPES at OW 128 and somewhat preferred the smoothing of details as presented in spectrograms obtained with BAPES at OW 32.

The ultrasound examination of today can potentially be improved if the conventional Welch's method for blood velocity estimation used in commercial scanners was replaced with one of adaptive spectral estimators BPC or BAPES. Consequently, either the temporal resolution of the spectrogram could be increased to obtain more information of the blood velocity profile, or the frame rate for the interleaved B-mode images could be increased to facilitate navigation under ultrasound examination. According to Gran et al. (2009), the adaptive methods are more computationally demanding than the conventional Welch's method, and BAPES is more computationally heavy than BPC. However, when reducing the OW, the computational costs decrease as well. Therefore, the BAPES method implemented with an OW 16 or the BPC method with an OW 32 may be as tractable as Welch's method with a much longer OW. It should therefore be possible to implement the methods into commercial scanners and convert the methods to an actual real-time modality.

Reproducibility of flow measurements

The storage time used from the experimental scanner RASMUS to the linux cluster and the off-line processing time used on

the cluster were considerable for each of the ultrasound methods investigated in study I-IV. It had two consequences for the study designs. Firstly, it had an impact on the logistics and reduced the number of samples that realistically could be enrolled into the study population, thereby affecting confidence intervals and limits of agreements of all the statistical calculations. Secondly, different days were used for examinations on the same volunteer. Although the volunteers rested 15 min before each scan, the flow dynamics, e.g. cardiac output, heart rate and stroke volume, were expected to fluctuate

For none of the four studies, the velocity estimation was repeated on the same volunteer with the same method. Furthermore, in study I and II where several methods estimated blood flow on the same volunteer, the examinations on each volunteer were accomplished within three weeks.

In study IV, inter- and intraobserver variability were assessed as tests for reproducibility. It was feasible as the experimental scanner RASMUS and the linux cluster already had produced the spectrograms, which were shown to the radiologists.

Therefore, tests of reproducibility of the flow measurements neither quantitative nor qualitative have been assessed. This would have required more observations along with the scans in comparison acquired simultaneously or within minutes. It will be a concern in future trials. It may be solved either by converting the methods into real-time estimation through commercial scanner implementation using dedicated processors or by implementing the methods into the new experimental scanner SARUS (Synthetic Aperture Real-time Ultrasound System), which is under development in CFU and will be able to acquire data much faster than the existing RASMUS scanner (148).

CONCLUSION AND PERSPECTIVES

Based on the *in-vivo* ultrasound studies on human volunteers presented in the thesis, it can be concluded that ultrasound vector flow and adaptive filtration have a number of advantages. The potentials in angle independent vector velocity techniques were investigated in study I-III. In study I and II, it was shown that *in-vivo* measurements of volume flow using the techniques Transverse Oscillation, Synthetic Transmit Aperture and Directional Beamforming were possible and that the estimates were in good agreement with magnetic resonance angiography. In study III, it was shown that *in-vivo* measurements of complex flow patterns in the cardiovascular system were possible with Plane Wave Excitation bringing forth novel information on fluid dynamics. Finally, it was shown that the optimization in frame rate and temporal resolution was possible. In study III, high frame rate was achieved with the vector velocity technique Plane Wave Excitation using plane wave emissions and in study IV high temporal resolution was achieved with the spectral Doppler techniques BAPES and BPC using adaptive filtration.

With vector velocity estimation, methods have been introduced to obtain quantitative blood flow measurements from the entire frame (and not only within a range gate), to estimate blood velocities in all vessels regardless of angle and to enable correct visualization of complex flow. Quantitative volume flow measurements obtained from the entire frame could be usable information when e.g. evaluating the severity of stenoses of the internal carotid artery, measuring cardiac output of the pulmonary artery/aorta or performing follow-up of transplanted organs. Additionally and perhaps mainly, vector velocity methods may uncover novel information of fluid dynamics. That is of complex flow patterns in simple and complex vessel geometries, secondary flow, vortices in bifurcations and around valves, and turbulence in the heart. Hence, vector velocity estimation could be a prognostic tool in the treatment of diseased vessels looking into altered flow patterns connected to e.g. venous insufficiency, atherosclerosis, tumor neovascularization or aneurysms.

With the adaptive spectral estimators BPC and BAPES and the vector velocity method Plane Wave Excitation is was shown that increased frame rate and temporal resolution can be achieved. The rapid temporal and spatial changes in blood flow especially in complex vessel geometries are crucial to understand and can be visualized with a high frame rate vector velocity method like Plane Wave Excitation. With the methods BPC and BAPES, solutions to increase the performance of spectral Doppler estimation were proposed. The results indicate that the adaptive methods BPC and BAPES potentially can bring improvements to spectral blood estimation as an increase of the temporal resolution of the spectrogram or as an increase of the frame rate for the interleaved B-mode images.

REFERENCE LIST

1. Jensen JA, Holm O, Jensen LJ, Bendsen H, Pedersen HM, Salomonsen K, et al. Experimental ultrasound system for real-time synthetic imaging. IEEE Ultrason Symp 1999;1595-9.
2. Jensen JA, Holm O, Jensen LJ, Bendsen H, Nikolov S, Tomov BG, et al. Ultrasound research scanner for real-time synthetic aperture image acquisition. IEEE Trans Ultrason Ferroelec Freq Contr 2005;52(5):881-91.
3. Caro CG, Pedley TJ, Schroter RC, Seed WA. The mechanics of the circulation. Oxford: Oxford University Press; 1978.
4. Griffiths PD, Hoggard N, Dannels WR, Wilkinson ID. In vivo measurement of cerebral blood flow: a review of methods and applications. Vasc Med 2001;6(1):51-60.
5. Masood S, Yang G-Z. Blood Flow Measurement. Encyclopedia of Biomedical Engineering. John Wiley & Sons, Inc.; 2005.
6. Headley JM. Invasive hemodynamic monitoring: physiological principles and clinical applications. Irvine: 2002.
7. Miles KA. Perfusion imaging with computed tomography: brain and beyond. Eur Radiol 2006 Nov;16 Suppl 7:M37-M43.
8. Ota H, Takase K, Rikimaru H, Tsuboi M, Yamada T, Sato A, et al. Quantitative vascular measurements in arterial occlusive disease. Radiographics 2005 Sep;25(5):1141-58.
9. Zaharchuk G. Theoretical basis of hemodynamic MR imaging techniques to measure cerebral blood volume, cerebral blood flow, and permeability. AJNR Am J Neuroradiol 2007 Nov;28(10):1850-8.
10. Turner J, Belch JJ, Khan F. Current concepts in assessment of microvascular endothelial function using laser Doppler imaging and iontophoresis. Trends Cardiovasc Med 2008 May;18(4):109-16.
11. Joyner MJ, Dietz NM, Shepherd JT. From Belfast to Mayo and beyond: the use and future of plethysmography to study blood flow in human limbs. J Appl Physiol 2001;91:2431-41.
12. Nair DG. About being BOLD. Brain Res Brain Res Rev 2005 Dec 15;50(2):229-43.
13. van der Geest RJ, Rob J, Niezen AR, van der Wall EE, de Roos A, Rieber JHC. Automated Measurement of Volume flow in the Ascending Aorta using MR Velocity Maps: Evaluation of

Inter- and Intraobserver Variability in Healthy Volunteers. J Comput Assist Tomogr 1998;22:904-11.
14. Split A, Box FMA, van der Geest, Reiber RJ, Kunz P, Kamper AM, et al. Reproducibility of total Cerebral Blood Flow Measurements Using Phase Contrast Magnetic Resonance Imaging. J Magn Reson Imaging 2002;16:1-5.
15. Oktar SO, Yucel C, Karaosmanoglu D, Akkan K, Ozdemir H, Tokgoz N, et al. Blood-flow volume quantification in internal carotid and vertebral arteries: Comparison of 3 different ultrasound techniques with phase-contrast MR imaging. AJNR Am J Neuroradiology 2006;27(2):363-9.
16. Ho SS, Chan YL, Yeung DK. Blood flow volume quantification of cerebral ischemia: comparison of three noninvasive imaging techniques of carotid and vertebral arteries. AJR Am J Roentgenol 2002;178:551-6.
17. Bakker CJ, Kouwenhoven M, Hartkamp MJ. Accuracy and precision of time-averaged flow as measured by non-triggered 2D phase-contrast MR angiography, a phantom evaluation. Magn Reson Imaging 1995;13:959-65.
18. Kondo C, Caputo GR, Semelka R, Foster E, Shimakawa A, Higgins CB. Right and left ventricular stroke volume measurements with velocity-encoded cine MR imaging: in vitro and in vivo validation. AJR Am J Roentgenol 1991 Jul;157(1):9-16.
19. Stahlberg F, Ericsson A, Nordell B, Thomsen C, Henriksen O, Persson BR. MR imaging, flow and motion. Acta Radiol 1992 May;33(3):179-200.
20. Graves MJ. Magnetic resonance angiography. Br J Radiol 1997 Jan;70:6-28.
21. Jensen JA. Medical ultrasound imaging. Prog Biophys Mol Biol 2007 Jan;93(1-3):153-65.
22. Jensen JA. Estimation of Blood velocities using ultrasound: A signal processing approach. New York: Cambridge University Press; 1996.
23. Tola M, Yurdakul M. Effect of Doppler angle in diagnosis of internal carotid artery stenosis. J Ultrasound Med 2006 Sep;25(9):1187-92.
24. Hoskins PR. Peak velocity estimation in arterial stenosis models using colour vector Doppler. Ultrasound Med Biol 1997;23(6):889-97.
25. Tortoli P, Michelassi V, Bambi G, Guidi F, Righi D. Interaction between secondary velocities, flow pulsation and vessel morphology in the common carotid artery. Ultrasound Med Biol 2003 Mar;29(3):407-15.
26. Ford MD, Xie YJ, Wasserman BA, Steinman DA. Is flow in the common carotid artery fully developed? Physiol Meas 2008 Nov;29(11):1335-49.
27. Hansen KL, Udesen J, Thomsen C, Jensen JA, Nielsen MB. In vivo validation of a blood vector velocity estimator with MR angiography. IEEE Trans Ultrason Ferroelec Freq Control 2009 Jan;56(1):91-100.
28. Frazin LJ, Lanza G, Vonesh M, Khasho F, Spitzzeri C, McGee S, et al. Functional chiral asymmetry in descending thoracic aorta. Circulation 1990 Dec;82(6):1985-94.
29. Lee KL, Doorly DJ, Firmin DN. Numerical simulations of phase contrast velocity mapping of complex flows in an anatomically realistic bypass graft geometry. Med Phys 2006 Jul;33(7):2621-31.
30. Steinman DA, Thomas JB, Ladak HM, Milner JS, Rutt BK, Spence JD. Reconstruction of carotid bifurcation hemodynamics and wall thickness using computational fluid dynamics and MRI. Magnet Reson Med 2002;47(1):149-59.
31. Zhao SZ, Xu XY, Hughes AD, Thom SA, Stanton AV, Ariff B, et al. Blood flow and vessel mechanics in a physiologically realistic model of a human carotid arterial bifurcation. J Biomech 2000;33(8):975-84.
32. Zhao SZ, Papathanasopoulou P, Long Q, Marshall I, Xu XY. Comparative study of magnetic resonance imaging and image-based computational fluid dynamics for quantification of pulsatile flow in a carotid bifurcation phantom. Ann Biomed Eng 2003;31(8):962-71.
33. Krams R, Bambi G, Giudi F, Helderman F, van der Steen AFW, Tortoli P. Effect of Vessel Curvature on Doppler Derived Velocity Profiles and Fluid Flow. Ultrasound Med Biol 2005;31:663-71.
34. Fei DY, Liu DD, Fu CT, Makhoul RG, Fisher MR. Feasibility of angle independent Doppler color imaging for in vivo application: Preliminary study on carotid arteries. Ultrasound Med Biol 1997;23(1):59-67.
35. Phillips DJ, Beach KW, Primozich J, Strandness DE, Jr. Should results of ultrasound Doppler studies be reported in units of frequency or velocity? Ultrasound Med Biol 1989;15(3):205-12.
36. Udesen J, Nielsen MB, Nielsen KR, Jensen JA. Examples of In Vivo Blood vector velocity Estimation. Ultrasound Med Biol 2007;33(4):541-8.
37. Cheng C, Tempel D, van Harperen R, van der Baan A, Grosveld F, Daermen M, et al. Atherosclerotic lesion size and vulnerability are determined by patterns of fluid shear stress. Circulation 2006;113(23):2744-53.
38. Richter Y, Edelman ER. Cardiology is flow. Circulation 2006;113(23):2679-82.
39. Vera N, Steinman DA, Ethier CR, Johnston KW, Cobbold RS. Visualization of complex flow fields, with application to the interpretation of colour flow Doppler images. Ultrasound Med Biol 1992;18(1):1-9.
40. Birchall D, Zaman A, Hacker J, Davies G, Mendelow D. Analysis of haemodynamic disturbance in the atherosclerotic carotid artery using computational fluid dynamics. Eur Radiol 2006;16(5):1074-83.
41. Hoskins PR. A review of the measurement of blood velocity and related quantities using Doppler ultrasound. Proc Inst Mech Eng [H] 1999;213(5):391-400.
42. Walker A, Olsson E, Wranne B, Ringqvist I, Ask P. Accuracy of spectral Doppler flow and tissue velocity measurements in ultrasound systems. Ultrasound Med Biol 2004 Jan;30(1):127-32.
43. Deane CR, Markus HS. Colour velocity flow measurement: in vitro validation and application to human carotid arteries. Ultrasound Med Biol 1997;23(3):447-52.
44. Stewart SF. Effects of transducer, velocity, Doppler angle, and instrument settings on the accuracy of color Doppler ultrasound. Ultrasound Med Biol 2001 Apr;27(4):551-64.
45. Gaitini D, Soudack M. Diagnosing carotid stenosis by Doppler sonography: state of the art. J Ultrasound Med 2005 Aug;24(8):1127-36.
46. Ranke C, Creutzig A, Becker H, Trappe H-J. Standardization of Carotid Ultrasound: A Hemodynamic Method to Normalize for Interindividual and Interequipment Variability. Stroke 1999;30:402-6.
47. Honish C, Sadanand V, Fladeland D, Chow V, Pirouzmand F. The reliability of ultrasound measurements of carotid stenosis compared to MRA and DSA. Can J Neurol Sci 2005;32(4): 465-471:-471.

48. Paivansalo MJ, Suramo I, Merikanto J, Lindholm EL. Interobserver, interequipment and intersubject variability of echo-Doppler examination of the common carotid and vertebral arteries. Eur J Ultrasound 1998 Apr;7(2):145-51.
49. Henry-Feugeas M, Kilic Genauzeau I, Ayme N, Schouman-Claeys E. Variability of ultrasonography velocity assessment of the carotid arteries. J Radiol 2000 Apr;81(4):445-9.
50. Daigle RE, Miller CW, Histand MB, McLeod FD, Hokanson DE. Nontraumatic aortic blood flow sensing by use of an ultrasonic esophageal probe. J Appl Physiol 1975;38:1153-60.
51. Fox MD. Multiple crossed-beam ultrasound Doppler velocimetry. IEEE Trans Son Ultrason 1978;25:281-6.
52. Trahey GE, Allison JW, Ramm OT. Angle independent ultrasonic detection of blood flow. IEEE Trans Biomed Eng 1987;34(12):965-7.
53. Bohs LN, Geiman BJ, Anderson ME, Gebhart SC, Trahey GE. Speckle tracking for multi-dimensional flow estimation. Ultrasonics 2000 Mar;38(1-8):369-75.
54. Newhouse VL, Censor D, Vontz T, Cisneros JA, Goldberg BB. Ultrasound Doppler probing of flows transverse with respect to beam axis. IEEE Trans Biomed Eng 1987;34:779-88.
55. Bonnefous O. Measurement of the complete (3D) velocity vector of blood flows. IEEE Ultrason Symp 1988;795-9.
56. Dunmire KW, Beach KW, Labs K-H, Plett M, Strandness DE. Cross-beam vector Doppler ultrasound for angle independent velocity measurements. Ultrasound Med Biol 2000;26:1213-35.
57. Overbeck JR, Beach KW, Strandness DE, Jr. Vector Doppler: accurate measurement of blood velocity in two dimensions. Ultrasound Med Biol 1992;18(1):19-31.
58. Kruskal JB, Newman PA, Sammons LG, Kane RA. Optimizing Doppler and color flow US: Application to hepatic sonography. Radiographics 2004;24(3):657-75.
59. Pozniak MA, Zagzebski JA, Scanlan KA. Spectral and color Doppler artifacts. Radiographics 1992 Jan;12(1):35-44.
60. Ferrara K, DeAngelis G. Color flow mapping. Ultrasound Med Biol 1997;23(3):321-45.
61. Stoica P, Moses R. Spectral analysis of signals. Upper Saddle River, N.J.: Prentice Hall; 2005.
62. Coats AJS, Murphy C, Conway J, Sleight P. Validation of the beat to beat measurement of blood velocity in the human ascending aorta by a new high temporal resolution Doppler ultrasound spectral analyser. Br Heart J 1992 Aug;68(8):223-9.
63. Tanaka N, Ohtsuki S. Estimation of Doppler shift frequency using selected phase information for high frame rate color flow mapping. J Med Ultrasonics 2004;31(1):5-12.
64. Udesen J, Gran F, Nielsen MB, Jensen JA. A Frequency Splitting Method for CFM Imaging. IEEE Ultrason Symp 2006;2019-22.
65. Gran F, Udesen J, Nielsen MB, Jensen JA. Coded ultrasound for blood flow estimation using subband processing. IEEE Trans Ultrason Ferroelec Freq Contr 2009;55(10):2211-20.
66. Oddershede N, Gran F, Jensen JA. Multi-frequency encoding for fast color flow or quadroplex imaging. IEEE Trans Ultrason Ferroelec Freq Control 2008 Apr;55(4):778-86.
67. Jensen JA. Spectral velocity estimation in ultrasound using sparse data sets. J Acoust Soc Am 2006;120(1):211-20.
68. Li J, Stoica P. An adaptive filtering approach to spectral estimation and SAR imaging. IEEE Trans Signal Process 1996;44(6):1469-84.
69. Herment A, Giovannelli JF. An adaptive approach to computing the spectrum and mean frequency of Doppler signals. Ultrason Imaging 1995 Jan;17(1):1-26.
70. Vaikus PJ, Cobbold RSC. A comparative study and assessment of Doppler ultrasound spectral estimation techniques, Part 1: Estimation methods. Ultrasound Med Biol 1988;14:661-72.
71. Vaikus PJ, Cobbold RSC, Johnston KW. A comparative study and assessment of Doppler ultrasound spectral estimation techniques, Part 2: Methods and results. Ultrasound Med Biol 1988;14:673-88.
72. Jensen JA, Munk P. A new method for estimation of velocity vectors. IEEE Trans Ultrason Ferroelec Freq Contr 1998;45:837-51.
73. Jensen JA. A new estimator for vector velocity estimation. IEEE Trans Ultrason Ferroelec Freq Contr 2001;48:886-94.
74. Udesen J, Jensen JA. Investigation of transverse oscillation method. IEEE Trans Ultrason Ferroelec Freq Contr 2006;53:959-71.
75. Jensen JA, Bjerngaard R. Directional velocity estimation using focusing along the flow direction: II: Experimental investigation. IEEE Trans Ultrason Ferroelec Freq Contr 2003;873-80.
76. Jensen JA. Directional velocity estimation using focusing along the flow direction: I: Theory and simulation. IEEE Trans Ultrason Ferroelec Freq Contr 2003;857-72.
77. Jensen JA. Field: A program for simulating ultrasound systems. Med Biol Eng Comp, vol 10th Nordic-Baltic Conference on Biomedical Imaging 1996;4:351-3.
78. Jensen JA, Svendsen NB. Calculation of pressure fields from arbitrarily shaped, apodized, and excited ultrasound transducers. IEEE Trans Ultrason Ferroelec Freq Contr 1992;39:262-7.
79. Holfort IK, Kortbek J, Jensen JA. In-vivo Vector Velocity Imaging Using Directional Cross-Correlation. IEEE Ultrason Symp 2006;2023-6.
80. Jensen JA. Velocity vector estimation in synthetic aperture flow and B-mode imaging. Proc IEEE Int Symp Biomed Imaging: from nano to macro 2004;1:33-6.
81. Jensen JA, Nikolov S. Transverse flow imaging using synthetic aperture directional beamforming. IEEE Ultrason Symp 2002;2:1488-92.
82. Jensen JA, Oddershede N. Estimation of velocity vectors in synthetic aperture ultrasound imaging. IEEE Trans Med Imag 2006;25:1637-44.
83. Nikolov S, Jensen JA. In-Vivo Synthetic aperture flow Imaging in Medical Ultrasound. IEEE Trans Ultrason Ferroelec Freq Contr 2003;50:848-56.
84. Oddershede N, Jensen JA. Experimental investigation of synthetic aperture flow angle estimation. Proc SPIE Med Imag 2005;5750:417-26.
85. Oddershede N, Jensen JA. Effects influencing focusing in synthetic aperture vector flow imaging. IEEE Trans Ultrason Ferroelec Freq Contr 2007;54:1811-25.
86. Udesen J, Gran F, Hansen KL, Jensen JA, Thomsen C, Nielsen MB. High frame-rate blood vector velocity imaging using plane waves: simulations and preliminary experiments. IEEE Trans Ultrason Ferroelec Freq Contr 2008;55(8):1729-43.
87. Udesen J, Gran F, Hansen KL, Jensen JA, Nielsen MB. Fast blood vector velocity imaging: Simulations and preliminary in vivo results. IEEE Ultrason Symp 2007;1005-8.
88. Friemel BH, Bohs LN, Trahey GE. Relative performance of two-dimensional speckle-tracking techniques: normalized

correlation, non-normalized correlation and sum-absolute-difference. IEEE Ultrason Symp 1995;2:1481-4.
89. Stoica P, Moses R. Introduction to spectral analysis. Upper Saddle River, N.J: Prentice Hall; 1997.
90. Gran F, Jakobsson A, Jensen JA. Adaptive spectral Doppler estimation. IEEE Trans Ultrason Ferroelec Freq Contr 2009;56(4):700-14.
91. Gran F, Jakobsson A, Jensen JA. Adaptive blood velocity estimation in medical ultrasound. Proc IEEE ICASSP 2007;1:293-6.
92. Stoica P, Jakobsson A, Li J. Matched-filterbank interpretation of some spectral estimators. Signal Processing 1998;66:45-59.
93. Proakis JG, Manolakis DG. Digital signal processing: Principles, algorithms and applications. 4. ed. Upper Saddle River, N.J.: Prentice Hall; 2007.
94. Chenevert TL, Fechner KP, Gelblum DY. Improvements in MR angiography using phase-corrected data sets. Magn Reson Med 1989 Apr;10(1):38-49.
95. Tublin ME, Bude RO, Platt JF. Review. The resistive index in renal Doppler sonography: where do we stand? AJR Am J Roentgenol 2003 Apr;180(4):885-92.
96. Altman DG. Practical statistics for medical research. London: Chapmann & Hall/CRC; 1991.
97. Landis JR, Koch GG. The measurement of observer agreement for categorical data. Biometrics 1977;33:159-74.
98. Fleiss JL. Measuring nominal scale agreement among many raters. Psychol Bull 1971;76(5):378-82.
99. Kim WY, Poulsen JK, Terp K, Staalsen NH. A new Doppler method for quantification of volumetric flow: in vivo validation using color Doppler. J Am Coll Cardiol 1996 Jan;27(1):182-92.
100. Kripfgans OD, Rubin JM, Hall AL, Gordon MB, Fowlkes JB. Measurement of volumetric flow. J Ultrasound Med 2006 Oct;25(10):1305-11.
101. Jenni R, Matthews F, Aschkenasy SV, Lachat M, van Der LB, Oechslin E, et al. A novel in vivo procedure for volumetric flow measurements. Ultrasound Med Biol 2004 May;30(5):633-7.
102. Soustiel JF, Levy E, Zaaroor M, Bibi R, Lukaschuk S, Manor D. A new angle-independent Doppler ultrasonic device for assessment of blood flow volume in the extracranial internal carotid artery. J Ultrasound Med 2002 Dec;21(12):1405-12.
103. Rothoerl RD, Schebesch KM, Woertgen C, Brawanski A. Ultrasonic blood flow volume assessment in the extracranial internal carotid artery in arteriovenous malformations. Neurol Res 2005 Mar;27(2):209-11.
104. Shuping GE, Liping BU, Honghai Z, Schelbert E, Disterhoft M. A Real-time 3-dimensional Digital Doppler Method for Measurement for Flow Rate and Volume Thorugh Mitral Valve in Children: A Validation Study Caompared With Magnetic Resonance Imaging. J Am Soc Echocardiogr 2005;18:1-7.
105. Forsberg F, Stein AD, Lui J, Deng X, Ackerman W, Herzog D, et al. Validating volume Flow Measurements from a Novel Semiautomated Four-dimensional Doppler Ultrasound Scanner. Acad Radiol 2006;13(10):1204-10.
106. Schrank E, Phillips DJ, Moritz WE, Strandness DE, Jr. A triangulation method for the quantitative measurement of arterial blood velocity magnitude and direction in humans. Ultrasound Med Biol 1990;16(5):499-509.
107. Steel R, Ramnarine KV, Davidson F, Fish PJ, Hoskins PR. Angle-independent estimation of maximum velocity through stenoses using vector Doppler ultrasound. Ultrasound Med Biol 2003 Apr;29(4):575-84.
108. Steel R, Ramnarine KV, Criton A, Davidson F, Allan PL, Humphries N, et al. Angle-dependence and reproducibility of dual-beam vector doppler ultrasound in the common carotid arteries of normal volunteers. Ultrasound Med Biol 2004 Feb;30(2):271-6.
109. Ricci S, Diciotti S, Francalanci L, Tortoli P. Accuracy and Reproducibility of a Novel Dual-Beam Vector Doppler Method. Ultrasound Med Biol 2008 Dec 23.
110. Fei DY, Fu CT. New method to obtain ultrasonic angle independent Doppler color images using a sector transducer. Ann Biomed Eng 1999 Mar;27(2):187-93.
111. Nyrnes SA, Lovstakken L, Torp H, Haugen BO. Blood flow imaging-a new angle-independent ultrasound modality for the visualization of flow in atrial septal defects in children. Echocardiography 2007 Oct;24(9):975-81.
112. Lovstakken L, Ibrahim KS, Vitale N, Henriksen ST, Kirkeby-Garstad I, Torp H, et al. Blood flow imaging: a new two-dimensional ultrasound modality for enhanced intraoperative visualization of blood flow patterns in coronary anastomoses. J Am Soc Echocardiogr 2008 Aug;21(8):969-75.
113. Pastorelli A, Torricelli G, Scabia M, Biagi E, Masotti L. A real-time 2-D vector Doppler system for clinical experimentation. IEEE Trans Med Imaging 2008 Oct;27(10):1515-24.
114. Ho SS, Metreweli C. Preferred technique for blood flow volume measurement in cerebrovascular disease. Stroke 2000 Jun;31(6):1342-5.
115. Powell AJ, Maier SE, Chung T, Geva T. Phase-velocity cine magnetic resonance imaging measurement of pulsatile blood flow in children and young adults: in vitro and in vivo validation. Pediatr Cardiol 2000 Mar;21(2):104-10.
116. Hundley WG, Li HF, Hillis LD. Quantitation of cardiac output with velocity-encoded, phase-difference magnetic resonance imaging. Am J Cardiol 1995;75:1250-5.
117. Rebergen SA, van der Wall EE, Doornbos J, de RA. Magnetic resonance measurement of velocity and flow: technique, validation, and cardiovascular applications. Am Heart J 1993 Dec;126(6):1439-56.
118. Lotz J, Meier C, Leppert A, Galanski M. Cardiovascular flow measurement with phase-contrast MR imaging: basic facts and implementation. Radiographics 2002 May;22(3):651-71.
119. Higginbotham MB, Morris KG, Williams S, McHale PA, Coleman RE, Cobb FR. Regulation of Stroke Volume during Submaximal and Maximal Upright Exercise in Normal Man. Circ Res 1986;58:281-91.
120. Polak JF. Peripheral Vascular Sonography: A Practical Guide. 2. ed. Lippincott Williams & Wilkins; 2004.
121. Oshinski JN, Curtin JL, Loth F. Mean-average wall shear stress measurements in the common carotid artery. J Cardiovasc Magn Reson 2006;8(5):717-22.
122. Brands PJ, Hoeks AP, Hofstra L, Reneman RS. A noninvasive method to estimate wall shear rate using ultrasound. Ultrasound Med Biol 1995;21(2):171-85.
123. Rubin JM. Spectral Doppler US. Radiographics 1994 Jan;14(1):139-50.
124. Friemel BH, Bohs LN, Nightingale KR, Trahey GE. Wall filtering challenges in two-dimensional vector velocity estimation. IEEE Ultrason Symp 1993;2:1031-4.
125. Oddershede N, Hansen KL, Nielsen MB, Jensen JA. In-vivo examples of synthetic aperture vector flow imaging. Proc SPIE Med Imag 2007;8:6510-3.

126. Marshall I, Papathanasopoulou P, Wartolowska K. Carotid flow rates and flow division at the bifurcation in healthy volunteers. Physiol Meas 2004 Jun;25(3):691-7.
127. Belz GG. Elastic properties and Windkessel function of the human aorta. Cadiovasc Drugs Ther 1995;9(1):73-83.
128. Qui Y, Quijano RC, Wang SK, Hwang HC. Fluid dynamics of venous valve closure. Ann Biomed Eng 1995;23(6):750-9.
129. Lurie F, Kistner RL, Eklof B, Kessler D. Mechanism of venous valve closure and role of the valve in circulation: A new concept. J Vasc Surg 2003;38(5):955-61.
130. Fisher J, Vaghaiwalla F, Tsitlik J, Levin H, Brinker J, Weisfleldt M, et al. Determinants and clinical significance of jugular venous valve competence. Circulation 1982;65(1):188-96.
131. Nedelmann M, Techner D, Dieterich M. Analysis of internal jugular vein insufficiency - a comparison of two ultrasound methods. Ultrasound Med Biol 2007;33(6):857-62.
132. Akkawi NM, Agosti C, Borroni B, Rozzini L, Magoni M, Vignolo LA, et al. Jugular valve incompetence: A study using air contrast ultrasonography on a general population. J Ultrasound Med 2002;21(7):747-51.
133. Shipkowitz T, Rodgers VGJ, Frazin LJ, Chandran KB. Numerical study on the effect of secondary flow in the human aorta on local shear stresses in abdominal aortic branches. J Biomech 2000;33(6):717-28.
134. Xue YJ, Gao PY, Duan Q, Lin Y, Dai CB. Preliminary study of hemodynamic distribution in patient-specific stenotic carotid bifurcation by image-based computational fluid dynamics. Acad Radiol 2008;49(5):558-65.
135. Schuierer G, Huk WJ. Diagnostic significance of flow separation within the carotid bifurcation demonstrated by digital subtraction angiography. Stroke 1990;21(12):1674-9.
136. Stokholm R, Oyre S, Ringgaard S, Flaagoy H, Paaske W, Pedersen EM. Determination of Wall Shear Rate in the Human Carotid Artery by Magnetic Resonance Techniques. Eur J Vasc Endovasc surg 2000;20(5):427-33.
137. Papathanasopoulou P, Zhao SZ, Kohler U, Robertson MB, Long Q, Hoskins P, et al. MRI measurement of time-resolved wall shear stress vectors in a carotid bifurcation model, and comparison with CFD predictions. J Magn Reson Imaging 2003;17(2):153-62.
138. Marshall I, Zhao S.Z., Papathanasopoulou P, Hoskins P, Xu XY. MRI and CDF studies of pulsatile flow in healthy and stenosed carotid bifurcation models. J Biomech 2004;37(5):679-87.
139. Timmers M, Wieling W, Karemaker JM, Lenders JWM. Denervation of carotid baro- and chemoreceptors in humans. J Physiol 2003;553(1):3-11.
140. Mancia G, Ferrari A, Gregorini L, Valentini R, Ludbrook J, Zanchetti A. Circulatory reflexes form carotid and extracarotid baroreceptor areas in man. Circ Res 1977;41:309-15.
141. Conley RB, Doux JD, Lee PY, Bazar KA, Daniel SM, Yun AJ. Integrating the theories of Darwin and Bernoulli: Maladaptive baroreceptor network dysfunction may explain the pathogenesis of aortic aneurysms. Med Hypotheses 2005;65:266-72.
142. Illig KA, Ouriel JA, Holen J, Green RM. Measurement of carotid birfurcation pressure gradients using the Bernoulli principle. J Vasc Surg 1996;4:130-4.
143. Henze L. In-vivo Vector Velocity Estimation Using Ultrasound, Masters Thesis. Copenhagen: Tehcnical University of Denmark; 2009.
144. Feng N, Zhang J, Wang W. An adaptive clutter rejection method based on AR model in color flow imaging. Ultrasonics 2006 Dec 22;44 Suppl 1:e85-e88.
145. Wang PD, Shen Y, Feng NZ. A novel clutter rejection scheme in color flow imaging. Ultrasonics 2006 Dec 22;44 Suppl 1:e303-e305.
146. Allam ME, Greenleaf JF. Isomorphism between pulsed-wave Doppler ultrasound and direction-of-arrival estimation - part I: Basic principles. IEEE Trans Ultrason Ferroelec Freq Contr 1996;43(5):911-22.
147. Allam ME, Kinnick RR, Greenleaf JF. Isomorphism between pulsed-wave Doppler ultrasound and direction-of-arrival estimation - part II: Experimental results. IEEE Trans Ultrason Ferroelec Freq Contr 1996;43(5):923-35.
148. Jensen JA, Hansen M, Tomov BG, Nikolov S, Holten-Lund H. System Architecture of an Experimental Synthetic Aperture Real-time Ultrasound System. IEEE Ultrason Symp 2007;636-40.